University of Nevada, Reno

Synthesis and Characterization of a Model Nickel Superoxide Dismutase Metallopeptide Functionalized for Hydrogen Production

A thesis submitted in partial fulfillment of the requirements for the degree of Master of Science in Chemistry

by

Bevan Griffith Meade

Dr. Jason Shearer/ Thesis Advisor

May, 2014

University of Nevada, Reno
Statewide • Worldwide

THE GRADUATE SCHOOL

We recommend that the thesis
prepared under our supervision by

BEVAN GRIFFITH MEADE

entitled

Synthesis And Characterization Of A Model Nickel Superoxide Dismutase Metallopeptide Functionalized For Hydrogen Production

be accepted in partial fulfillment of the
requirements for the degree of

MASTER OF SCIENCE

Jason M. Shearer, Ph.D., Advisor

Brian J. Frost, Ph.D., Committee Member

R. George Scott, Ph.D., Graduate School Representative

Marsha H. Read, Ph. D., Dean, Graduate School

May, 2014

Abstract

Hydrogenases (H_2ase) are naturally occuring enzymes that reversibly catalyze the oxidation and production of H_2 from protons at low overpotential with very high catalytic activity. As a result these enzymes have gained increased attention over recent years as potential models for technological materials in the industrial production of hydrogen as a stock fuel. Despite the many attempts to replicate the properties of these enzymes synthetically, very few synthetic models have shown catalytic activity comparable to that of the native enzyme. This project seeks to utilize key features from the coordination environment selected by nature for the seemingly unrelated NiSOD (nickel-superoxide dismutase) metalloenzyme to produce a biological mimic of [NiFe]H_2ase. A metallopeptide consisting of the 12 *N*-terminal residues from the NiSOD primary sequence, which has been extensively studied by the Shearer group, was used as the basis for constructing this mimic because it is a structurally and mechanistically well-defined system. Careful consideration of the requirements necessary for nickel coordination to the NiSOD apopeptide and the influence of structure on the reactivity of the nickel containing metallopeptide provided a guide for its modification resulting in properties that may be useful in the construction of an H_2ase active metallopeptide. Substitution of the *N*-terminal histidine residue with the phosphine PTA (1,3,5-triaza-7-phosphatricyclo[3.3.1.1]decane) is proposed to optimize the active site of this enzyme toward H_2 production while maintaining redox activity and stability. The synthesis and characterization by nuclear magnetic resonance, electronic absorption and X-ray absorption spectroscopy of this modified maquette are reported herein. It will be shown that this novel metallopeptide [Ni(H_2ase^{M1})] contains Ni^{II} in square pyramidal environment with ligands derived from the PTA (P atom), Cys(2) and Cys(6) (S atoms), the Cys(2)

amidate (N atom) and water (H_2O). Further studies of this system will be aimed at understanding the functional properties of the metallopeptide as a hydrogenase.

Acknowledgements

I would like to thank Prof. Jason Shearer for all of his guidance over the course of my graduate work and for all of his support in the writing and defense of my thesis. Additionally I would like to thank my committee members Prof. Brian Frost and Prof. R. George Scott for their time, helpful suggestions and corrections to my thesis. I would also like to thank my group members Kristy Peck, Jennifer Schmitt, Paige Callan-Wickum, Kyle Rosenkoetter, Jamie Schwarzbach and Heather Clewett for all of their advice, support and friendship in the lab. I would like to thank the chemistry office staff Roxie Taft, Jennifer Heck and Xanthia Elsbree for all of their help and support in my academic pursuits in the chemistry department. Additionally I would like to thank the UNR Chemistry Department for the opportunity to further my studies and fellow graduate students for their support and friendship during my graduate studies.

Finally, I would like to express my endless gratitude toward my parents, sister and wonderful wife for their love, encouragement, patience and inspiration.

Table of Contents

List of Figures

List of Abbreviations

AA	amino acid
CD	circular dichroism
DCM	dichloromethane
DIC	*N,N*'-Diisopropylcarbodiimide
DIEA	*N,N*'-Diisopropylethylamine
DMAP	4-dimethylaminopyridine
DMF	dimethylformamide
DMSO	dimethyl sulfoxide
EDC	1-ethyl-3-(3-dimethylaminopropyll) carbodiimide
EDT	1,2-ethanedithiol
EPR	electron paramagnetic resonance
ESI	electrospray ionization spectrometry
EXAFS	X-ray absorption far edge spectroscopy
Fmoc	9-fluoroenylmethoxycarbonyl
FT	Fourier transform
{H_2ase^{M1}}	PTA-CDLPC-GVYDP-A-COOH
{H_2ase^{M2}-Asp}	PTA-CDLPC-GVYDP-A(D)-COOH
{H_2ase^{M2}-Lys}	PTA-CDLPC-GVYDP-A(K)-COOH
HBTU	*O*-(Benzotriazole-1-yl)-*N,N,N',N'*-tetramethyluronium hexafluorophosphate
HOBt	hydroxybenzotriazole
HPLC	high performance liquid chromatography
NEM	*N*-ethylmorpholine
{$Ni^{II}(H_2ase^{M1})$}	$[Ni\text{-}(PTA\text{-}CDLPC)(\text{-}GVYDP\text{-}A\text{-}COOH)]^{2+}$
{$Ni^{II}(H_2ase^{M2}$-Asp)}	$[Ni\text{-}(PTA\text{-}CDLPC)(\text{-}GVYDP\text{-}A(D)\text{-}COOH)]^{2+}$
{$Ni^{II}(H_2ase^{M2}$-Lys)}	$[Ni\text{-}(PTA\text{-}CDLPC)(\text{-}GVYDP\text{-}A(K)\text{-}COOH)]^{2+}$
NHS	*N*-hydroxysuccinimide
NiSOD	nickel superoxide dismutase
NMP	*N*-methyl-2-pyrrolidone
NMR	nuclear magnetic resonance
PTA	1,3,5-triaza-7-phosphatricyclo[3.3.1.1]decane
PTA-COOLi	lithium 1,3,5-triaza-7-phosphaadamantane-6-carboxylate
ROS	reactive oxygen species
SOD	superoxide dismutase
SPPS	solid-phase peptide synthesis
TFA	trifluoroacetic acid
UV-Vis	ultraviolet-visible
XANES	X-ray absorption near-edge structure
XAS	X-ray absorption spectroscopy

Amino Acids

A	alanine (Ala)
C	cysteine (Cys)
D	aspartic acid (Asp)
E	glutamic acid (Glu)
F	phenylalanine (Phe)
G	glycine (Gly)
H	histidine (His)
I	isoleucine (Ile)
K	lysine (Lys)
L	leucine (Leu)
M	methionine (Met)
N	asparagine (Asn)
P	proline (Pro)
Q	glutamine (Gln)
R	arginine (Arg)
S	serine (Ser)
T	threonine (Thr)
V	valine (Val)
W	tryptophan (Trp)
Y	tyrosine (Tyr)

Chapter 1

Native [NiFe] Hydrogenase and Functional Mimics

1.1 Introduction

Many organisms utilize molecular hydrogen as a reducing currency as well as a source of protons for various cellular processes. The enzymes that facilitate proton reduction and hydrogen oxidation are known as hydrogenases (H_2ase) (Eqn. 1.1) and fall into one of three categories based on the active metal site: binuclear NiFe ([NiFe]H_2ase) and FeFe ([FeFe]H_2ase) or mononuclear Fe ([Fe]H_2ase).[1]

Equation 1.1: $2H^+ + 2e^- \rightleftharpoons H_2$

In addition to a low-spin iron center, the ligation of sulfur ligands to the active site is a common feature. The reversibility of the reaction in Eqn. 1.1 is another hallmark of H_2ase and is dependent on both the location of the native enzyme within the cell and the local pH.

The ability of H_2ases to reversibly catalyze the production of H_2 has made them an attractive area of study in the development of catalysts for hydrogen fuel cells, which utilize H_2 as a fuel source and couple the reduction of resulting protons with O_2 to generate H_2O.[1-3] The finite supply of petroleum feedstock makes alternative sources of energy an ever increasing necessity and the prospect of a H_2 economy has long been considered and explored as a cheap method for the chemical storage of energy. Presently, H_2 is derived primarily from fossil fuels employing relatively high energy processes accompanied by significant production of greenhouse gases.[4] It has thus been suggested that hydrogen be viewed as an indirect “energy currency” rather than a direct replacement for fossil fuels.[5,6] The large scale splitting of water

has subsequently become a Holy Grail in the search for a clean, cheap and efficient source of hydrogen.[7] Current platinum catalysts are able to facilitate the production of hydrogen. However, due to the low Earth abundance of platinum and its high demand outside the realm of hydrogen chemistry, these catalysts are unsustainable for use in H_2 production on a global scale.[8] In the wide search for a low-cost and efficient alternative many have turned their attention to H_2ase enzymes. The redox properties of these enzymes have been finely tuned by nature to allow the oxidation and production of H_2 without requiring a large overpotential, or driving force in excess of the thermodynamically predicted redox potential. The added advantages of incorporating first-row transition metal centers into the active sites has made the prospect of producing catalysts based on H_2ase enzymes an attractive alternative to current methods of H_2 production.[2]

1.2 [NiFe]Hydrogenase

Before H_2ase -inspired materials can be made, the nature of the active site at which hydrogen chemistry occurs must be adequately understood. Lessons learned from the study of H_2ases could then be utilized to guide the production of H_2-producing molecular catalysts. In the native [NiFe]H_2ase enzyme the active site is anchored to the protein through four cysteine thiolates, two of which bind to nickel terminally while the other two provide bridging sulfurs between the Ni and Fe centers, resulting in a distorted square planar environment about the nickel center. Additionally the iron atom exhibits three diatomic strong field ligands assigned as CO and two CN^-(Fig. 1.1).[1-3,7,9] Initial X-ray crystallographic studies of the native enzyme indicated a hydrophobic channel through which substrates are transported to and from the active site while electron transfer occurs through a chain of [Fe_4S_4] clusters. The end of this tunnel was observed to be in close proximity to an open coordination site on the nickel atom,

suggesting that substrate binding occurs at or near the nickel center instead of the proximal iron atom.[1-3] Electron paramagnetic resonance (EPR) studies provide further evidence for a redox-active nickel center and an EPR-silent iron (II) center in the active site for a variety of enzymatic states. This implicates nickel as the site for substrate binding and redox.[3,7,9] Despite the well characterized structural features of the native enzyme, the mechanism by which the oxidation and production of H_2 is achieved is much less understood. This is evidenced by a plethora of structural and redox states of the enzyme including inactive, active, "ready", and "unready" states which have been spectroscopically characterized. These differ in metal-center oxidation states, metal-center coordination geometries and ligands coordinated to the metal centers and their individual mechanistic relevance are a matter of debate.[2,3,9]

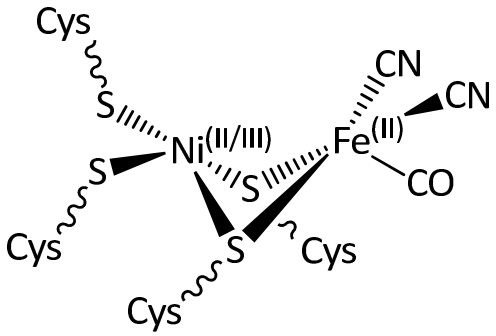

Figure 1.1 Native [NiFe]H_2ase active site.

1.3 [NiFe]Hydrogenase Models

Many model compounds have been synthesized to further understand the nature of the active site and the mechanism by which [NiFe]H_2ase] enzymes facilitate H_2 production and oxidation.[3,6,10,12-17] There are two driving forces for the synthesis of model compounds. The first is a biomimetic approach, which aims to better understand the active site and potential intermediate species of the native enzyme. The second is a "bio-inspired" approach, which

involves synthesis of catalysts with the potential to replicate the native enzyme on an industrial scale. The former approach involves the synthesis of models that mimic the structure of the active site so that the spectroscopic, electronic structure and structural properties can be quantified and compared with their ability to catalyze the oxidation and production of H_2.[2,3] These studies have shed light on the structure/function relationships within the active site and have laid the foundation for possible mechanisms. Many structural variations of the [NiFe]H_2ase active site have been synthesized over the past few decades. Structural models that best replicate the native [NiFe]H_2ase active site have been provided by the Tatsumi group and feature similar metal-metal and metal sulfur distances as well as low spin Ni(II) and Fe(II) centers (Fig. 1.2).[3,14,18-20] The vast majority of these structural analogues, however, have shown little or no reactivity toward H_2 oxidation or production and fewer still have shown any catalytic activity.[3]

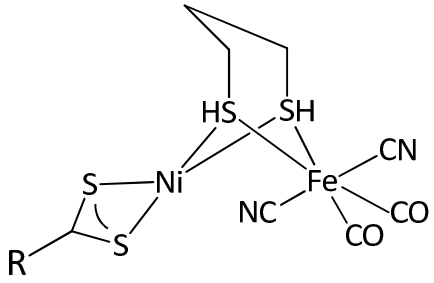

Figure 1.2 Structural Model of the [NiFe]H_2ase] active site [R = $N(Et)_2$, $N(C_5H_{10})$].[20]

A recent study[21] by the Varganov group probed the influence of varying the geometric structure of the [NiFe]H_2ase active-site. Specifically, the nature of the distorted geometry of the coordination environment in the native [NiFe]H_2ase active site, which is set between square planar and tetrahedral, and its relationship to the spin state of the nickel center were investigated. This unusual geometry is enforced by the protein matrix, and places the active site

into what is called an “entatic state”, or activated-state a term coined by Vallee and Williams in 1968 to describe unique coordination environments affected by the protein architecture.[22] *Ab initio* computational modeling of the active site was performed and the calculated energy for multiple geometries was compared with changes in a dihedral angle (⍰) describing the NiS_4 metal-center. Rotation of the terminal thiolate ligands about the nickel center relative to the bridging thiolate ligands effected the change in this dihedral angle (Fig. 1.3) while the relative energies of each geometry were calculated at the PBE/def2-TZPD//PBE/bs1 level of theory. It was found that as the dihedral angle of the square planar model was increased (from 0°) and that of the tetrahedral model was decreased (from 90°) it was observed that an overlap in calculated energies occurs at a dihedral angle near 70°. It was observed that the resulting twisted tetrahedral geometry closely resembles that of the native active site and was proposed to allow the redox active molecular orbital (RAMO) the ability to “hop” between quasi-degenerate singlet and triplet states, optimizing catalysis. This might explain the lack of activity in many structural models that adopt rigorous square planar geometries about the nickel center.[21]

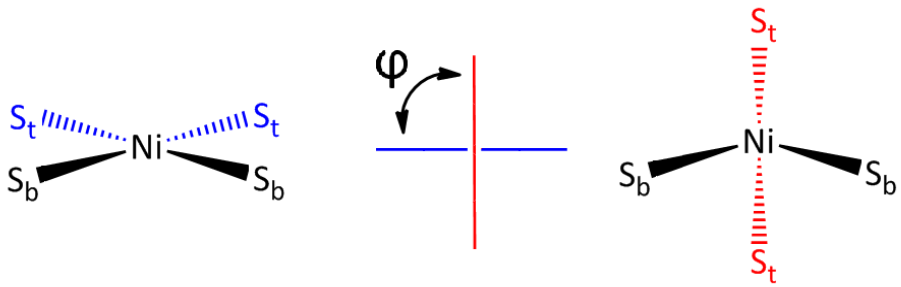

Figure 1.3 Dihedral angle upon rotation of terminal thiolates about the nickel center.

1.3.1 Functional [NiFe] Hydrogenase Models

Many model compounds that structurally resemble [NiFe]H_2ase have led shed some light on the nature of the native enzyme, including investigations of metal-metal distances and thiolate ligand dihedral angles[23], the role of variable geometries in dihydrogen activation[24], and the role of thiolate protonation[25,26]. Despite the widespread synthesis of structural models, those with the capacity to produce or oxidize H_2 catalytically are few and far between[3,25]. The synthesis of functional analogues with the sole objective of reproducing the reaction within the active site, rather than its structure, has led to a number of successes.[3,27-30] The approach taken to produce functional models provides the potential for the reaction to be scaled up upon removal of the inherent constraints of a physiological environment.[10]

DuBois illustrates an ideal functional H_2ase as a catalyst that lowers activation energies while maintaining a small ΔG° between intermediates to avoid multiple high energy activation barriers. This is demonstrated by comparison of a moderate catalyst (red) and an ideal catalyst (blue) (Fig 1.4). In the case of a H_2ase cell the overpotential can be defined as the difference between the potential at which catalysis occurs and the standard potential for the half reaction involving a proton source, such as a weak acid (HA), and H_2.[10]

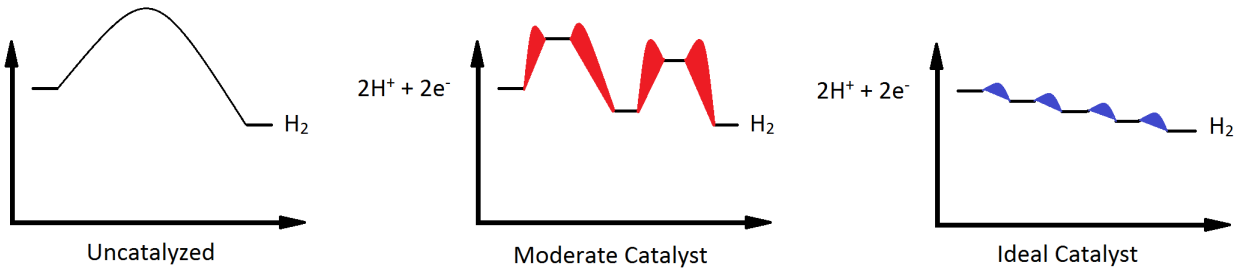

Figure 1.4 Reaction coordinate diagrams for catalyzed H_2 production.

1.3.2 [NiRu]-Based Hydrogenase Models

Ogo and co-workers recently developed a [NiRu] binuclear metal complex that behaves as a functional model of the [NiFe] active site.[13,27,31-33] The primary structural changes observed in the mimic relative to the [NiFe]H_2ase active site are the replacement of the Fe atom with an isoelectronic Ru atom to allow formation of stable aqua complexes. The inclusion of an aqua ligand has been implicated in aiding the formation of metal-hydride species (Fig. 1.5). The chelating N_2S_2 ligand set forces a square planar geometry, stabilizes higher nickel oxidation states and avoids risk of thiolate oxidation relative to the labile NiS_4 motif found in the native active site.[34] Additionally the μ-thiolato moieties enforce small bite angles to accommodate bridging hydride species. The hexamethyl benzene (HMB) ligand was also included to mimic the electronic nature of the Fe-CO/CN ligand set.[27]

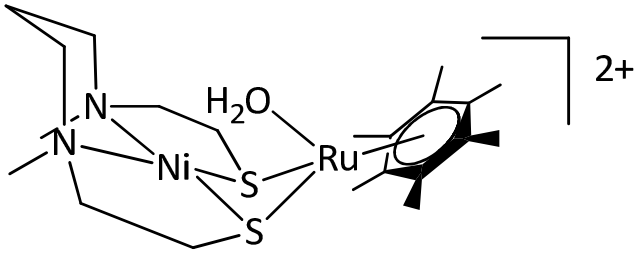

Figure 1.5 Functional {[NiRu]H_2ase} model.[27]

Mechanistic studies (Fig. 1.6) of the [NiRu]suggest an initial heterolytic cleavage of H_2 to form the coordinated hydride. This is followed by the cleavage of a second H_2 to afford a proposed dihydride species and loss of a second proton. Reductive elimination results in the loss of H_2 and the oxidation state of the complex remains reduced by the two remaining electrons. This is confirmed by the observed reduction of $CuSO_4$ to Cu^0 and regeneration of the initial active catalyst, yielding an overall oxidation of one H_2 molecule to two protons and two electrons.[27]

The main difference in reactivity between this complex and the native [NiFe]H_2ase active site is the involvement of both metal centers in the redox chemistry taking place. The formation of a metal-metal bond and reduction in oxidation state of the metals is proposed to provide temporary storage for two electrons until an oxidizing agent (in this case Cu^{2+}) presents itself.

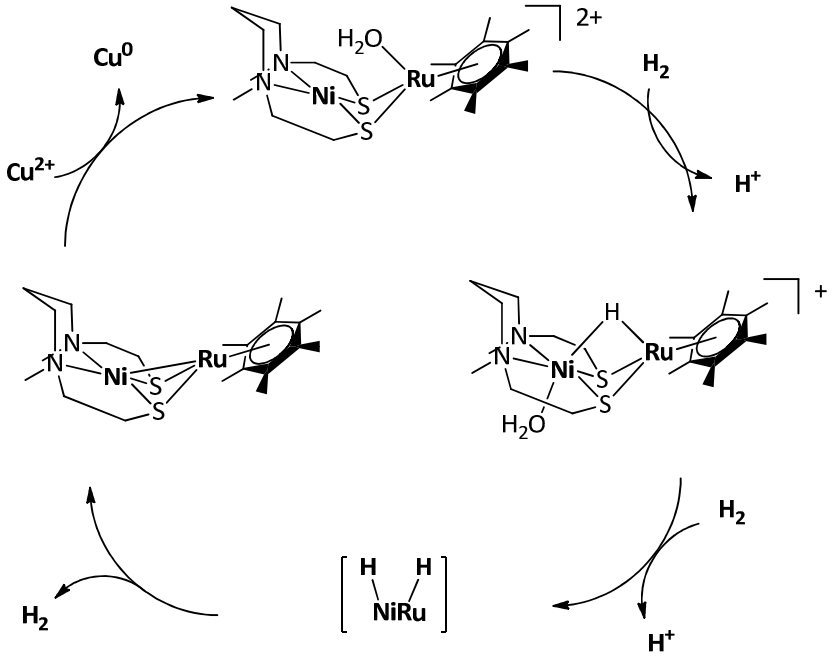

Figure 1.6 Proposed mechanism for H_2 oxidation by a {[NiRu]H_2ase} model.[27]

A recent study by Artero and Fontecave provides indirect evidence for an intramolecular proton-coupled electron-transfer (PCET) event in a [NiRu] mimic similar to that of Ogo and coworkers. [11] The structural changes made to Ogo's complex[27] included the replacement of the aqua ligand with a chloride ligand and the replacement of propanediamino ligand with benzyldithiolate. Bulk electrolysis experiments of this complex were conducted in DMF (vs. Fc^+/Fc) in the presence of the strong and weak acids trifluoroacetic acid (TFA) (0.95 mM complex) and triethyl ammonium $(Et_3NH)^+$ (2.0 mM complex), respectively. Subsequent DFT modeling of reaction intermediates allowed the generation of a mechanistic scheme (Fig. 1.7),

which includes the calculated reaction enthalpies (kJ mol^{-1}) and redox potentials (V vs Fc^{+}/Fc) for each step. This allows comparison of the ability for metal-hydride species to form in the presence of strong and weak proton donors.

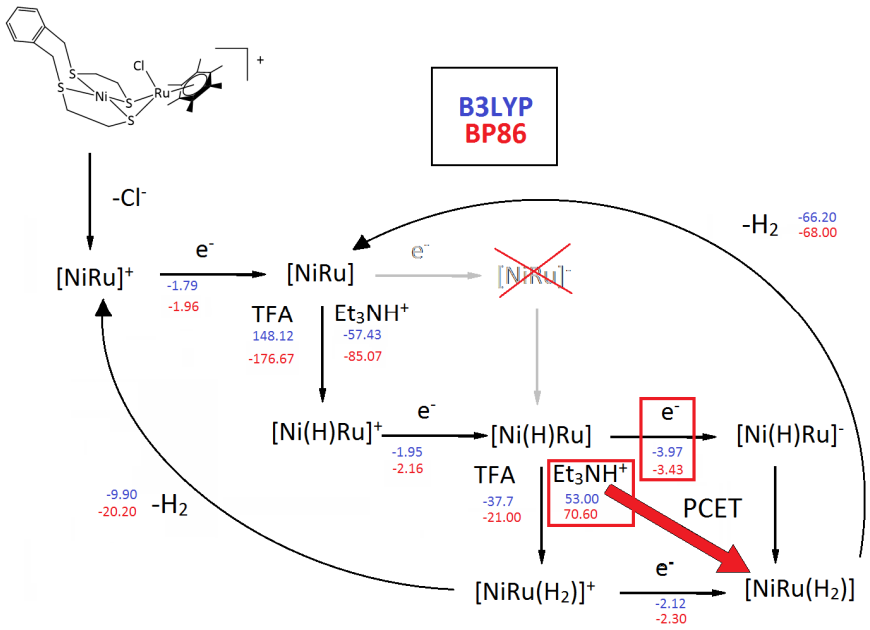

Figure 1.7 Mechanistic scheme for H_2 production by a {[NiRu]H_2ase} model in the presence of TFA and $(Et_3NH)^{+}$. Calculated eaction enthalpies for protonation steps (kJ mol^{-1}) and redox potentials (V vs Fc/Fc^{+}) are given in blue (B3LYP) and red (BP86) for each step.[11]

In both cases elimination of the chloride ligand was observed followed by protonation and subsequent reduction yielding the hydride species. In the presence of TFA this complex was unable to undergo further reduction because of an exceedingly negative potential and discrete protonation followed by reduction at a lower potential was observed. The resulting dihydride species underwent reductive elimination to afford the cationic $[NiRu]^{+}$ species and H_2 upon recycling. In the presence of $Et_3NH_4^{+}$ the hydride species was again formed by protonation and subsequent reduction. The formation of the dihydride species could not proceed through protonation owing to the positive reaction enthalpies associated with the acid; $Et_3NH_4^{+}$ is too

weakly acidic to drive the reaction. The experimentally derived negative reduction potential also made initial formation of the anionic species very unlikely. However, H_2 formation was still observed in bulk electrolysis experiments using a mercury pool cathode, leading to the conclusion that a PCET event may be a more thermodynamically favorable pathway to the dihydride species although the exact mechanistic nature of the PCET event was not explicitly defined .[11]

1.3.3 Mononuclear [Ni] Hydrogenase Model

The mononuclear nickel H_2ase complexes prepared by DuBois and coworkers is at the forefront of bio-inspired hydrogen-production molecular catalysts (Fig. 1.8).[10,17] The careful design of this catalyst relies on the minimization of ΔG° between intermediates and allows for both the oxidation and production of H_2. This is accomplished by inclusion of pendant amine proton donor/acceptor moieties which can be fine-tuned to facilitate intramolecular proton exchange between the metal center and solution. This is dependent on the basicity of the amine which can be adjusted by increasing or decreasing the electron withdrawing ability of R'. Decreased basicity allows the amine better proton donor ability, biasing catalysis toward H_2 production. Conversely a more basic amine will more readily abstract a proton from coordinated H_2, resulting in heterolytic cleavage.[12,29]

Incorporation of a chelating phosphine ligand sphere allows tuning of the hydride donor/acceptor ability (or "hydricity") of the nickel center. The hydricity of the metal ΔG°(H^-) can be fine-tuned by adjusting the stearic bulk of bidentate phosphine ligands about the metal to induce distortion of the ligand set toward a more tetrahedral geometry. This has been found to lower the energy of the LUMO, which is the acceptor orbital for hydride electrons.

Additionally, incorporation of a more electron withdrawing R group results in a metal better suited for accepting a hydride and a better catalyst for H_2 production.[29]

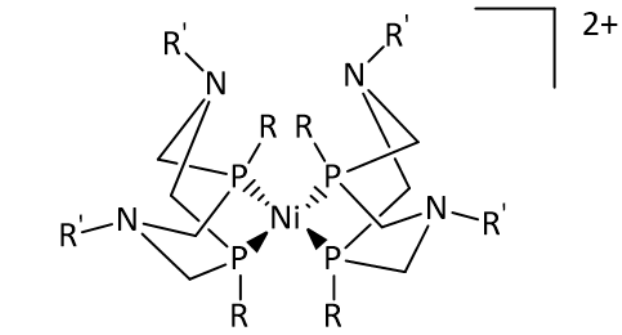

Figure 1.8 Functional Mononuclear {[Ni]H_2ase} model.[17]

The mechanism (Fig 1.9) by which this complex is proposed to catalyze the oxidation and production of H_2 involves the shuttling of protons by pendant amines to and from the nickel center accompanied by transitions between Ni(II), Ni(I) and Ni(0) oxidation states. For the production of H_2 the cycle begins with reduction of Ni(II) to Ni(I) followed by protonation of a pendant amine. DuBois and coworkers suggest that electron density is drawn away from the metal center to stabilize this protic species. Simultaneous reduction of the metal coupled upon transfer of a proton from the pendant amine results in the Ni(II)-hydride species. This step is suggested to occur in order to avoid the formation of a high energy Ni(III)-hydride species and demonstrates the utility of internal bases.[29] Protonation of another pendant amine yields the spectroscopically observed diprotonated species in which both amines are protonated and the

electrons are stored in the Ni(0) center. This is followed by formation of a Ni(II)-H_2 species which, upon elimination of H_2, regenerates the initial Ni(II) complex.[10,17,29]

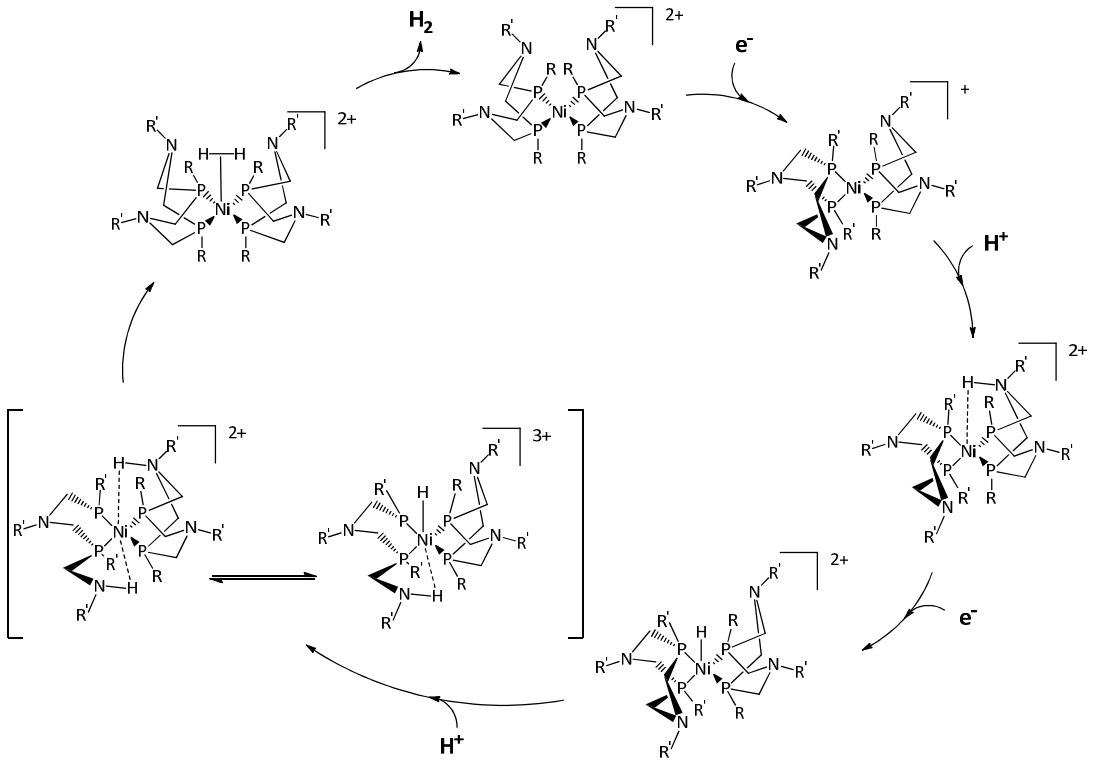

Figure 1.9 Mechanism for H_2 production by a mononuclear {[Ni]H_2ase} model involving proton transfer upon reduction.[29]

DuBois and coworkers later introduced another mononuclear catalyst with minimal structural changes and marked improvements in catalytic performance. The new catalysts incorporates only two pendant amines where the first generation employed four, leading to endo-/exo- isomerization which inhibits turnover (1040 s^{-1}). Similar structural changes were not observed in the newer version and turnover frequencies were measured up to 106,000 s^{-1} in solutions with 1.2 M H_2O. However, this complex exhibited a large overpotential of 625 mV (vs Fc^+/Fc) in comparison to the original catalyst (290 mV vs Fc^+/Fc) making it unviable for H_2

production. For the sake of comparison, [FeFe] hydrogenase displays a TOF around 9000 s^{-1} with an overpotential <100 mV.[28,30]

1.4 Summary

Evaluation of these functional H_2ase models has provided some criteria with which to examine the possibility of functionalizing the nickel superoxide dismutase (NiSOD) active site for H_2 production. As will be demonstrated in Chapter two, the coordination motif within Ogo's [NiRu] model shares many similarities with that of nickel superoxide dismutase (NiSOD) including mixed N_2S_2 coordination to allow oxidative protection to sulfur ligands as well as a chelating ligand sphere. The nickel complex put forth by DuBois and coworkers demonstrates that H_2ase properties can be achieved in mononuclear Ni-compounds and highlights the use of pendant amines to bring protons within close proximity of the metal center. Upon observation of both functional [NiFe]H_2ase mimics, it is evident that internal bases play a key role in directing protons to the metal center while avoiding high-energy intermediates and subsequently high overpotentials. The role of coordinated sulfurs as proton sources within the NiSOD coordination environment will also be discussed in chapter two. Additionally the role of mixed NiN_2S_2 ligand sphere in protecting thiols and providing stabilization to the Ni-center will be discussed.

1.5 References

1) (a) Fontecilla-Camps, J. C.; Volbeda, A.; Cavazza, C.; Nicolet, Y. *Chem. Rev.* **2007**, *107*, 4273-4303
(b) Collman, J. P. *Nat. Struct. Biol.* **1996**, *3*, 213-217
(c) Bagley, K. A.; Van Garderen, C. J.; Chen, M.; Duin, E. C.; Albracht, S. P.; Woodruff, W. H. *Biochemistry* **1994**, *33*, 9229-9236
(d) Bagley, K. A.; Duin, E. C.; Roseboom, W.; Albract, S. P. J.; Woodruff, W. H. *Biochemistry*, **1995**, *34*, 5527-5535
(e) Happe, R. P.; Roseboom, W.; Pierik, A. J.; Albracht, S. P. J.; Bagley, K. A. *Nature*, **1997**, *385*, 126

2) (a) Fontecilla-Camps, J. C.; Amara, P.; Cavazza, C.; Nicolet, Y.; Volbeda, A. *Nature* **2009**, *460*, 814-822
(b) Voldbeda, A.; Charon, M.; Piras, C.; Hatchikian, E. C.; Frey, M.; Fontecilla-Camps, J. C. *Nature* **1995**, *373*, 580-587
(c) Ogata, H.; Mizoguchi, Y.; Mizuno, N.; Miki, K.; Adachi, S.; Yasuoka, N.; Yagi, T.; Yamauchi, O.; Hirota, S.; Higuchi, Y. *J. Am. Chem. Soc.* **2002**, *124*, 11628-11635

3) Pickett, C. J.; Tard, C. *Chem. Rev.* **2009**, *109*, 2245-2274

4) Muradov, N. Z.; Veziroglu, T. N. *Int. J. Hydrogen Energy* **2005**, *30*, 225-237

5) Lubitz, W.; Tumas, W. *Chem. Rev.* **2007**, *107*, 3900-3903

6) Heinekey, D. M. *J. Organometallic Chem.* **2009**, *694*, 2671-2680

7) (a) Lubitz, W.; Reijerse, E.; van Gastel, M. *Chem. Rev.* **2007**, *107*, 4331-4365
(b) Kubas, G. J. *Chem. Rev.* **2007**, *107*, 4152-4205
(c) Lubitz W.; van Gastel, M.; Gaertner, W. *Met. Ions Life Sci.* **2007**, *2*, 279-322

8) Berger, D. J. *Science*, **1999**, *286*, 49

9) Lubitz, W.; Pandelia, M.; Ogata, H. *ChemPhysChem*, **2010**, *11*, 1127-1140

10) Gloaguen, F.; Rauchfuss, T. B. *Chem. Soc. Rev.* **2009**, *38*, 100-108

11) (a) Artero, V.; Canaguier, S., Fourmond, V.; Perotto, C. U.; Fize, J.; Pecaut, J.; Fontecave, M.; Field, M. J. *Chem. Comm.* **2013**, *49*, 5004-5006
(b) Artero, V.; Fontecave, M.; Canaguier, S.; Field, M.; Oudart, Y.; Pecaut, J. *Chem. Comm.* **2010**, *46*, 5876-5878

12) Bullock, R. M.; DuBois, D. L. *Eur. J. Inor. Chem.* **2011**, 1017-1027

13) Ogo, S. *Science* **2007**, *316*, 585-587

14) Tatsumi, K.; Ohki, Y. *Eur. J. Inorg. Chem.* **2011**, 973-985

15) Bouwman, E.; Reedijk, J. *Coord. Chem. Rev.* **2005**, *249*, 1555-1581

16) Artero, V.; Fontecave, M.; Canaguier, S. *Dalton Trans.* **2008**, 315-325

17) DuBois, D. L.; DuBois, M. R.; Wilson, A. D.; Newell, R. H.; McNevin, M. J.; Muckerman, J. T. *JACS* **2006**, *128*, 358-366

18) Tatsumi, K.; Tanino, S.; Li, Z.; Ohki, Y. *Inorg. Chem.* **2009**, *48*, 2358-2360

19) Tatsumi, K.; Ohki, Y.; Yasumura, K.; Kuge, K.; Tanino, S.; Ando, M.; Li, Z. *PNAS* **2008**, *105*, 7652-7657

20) Tatsumi, K.; Li, Z.; Ohki, Y. *JACS* **2005**, *127*, 8950-8951

21) Varganov, S. A.; Yson, R. L.; Gilgor, J. L; Guberman, B. A. *Chem. Phys. Lett.* **2013**, *577*, 138-141

22) Williams, J. P.; Vallee, B. L. *Proc. Natl. Acad. Sci.* **1968**, *59*, 498-505

23) Zhu, W. F.; Mar, A. C.; Wang, Q.; Neese, F.; Spencer, D. J. E.; Blake, A. J.; Cooke, P. A.; Wilson C.; Schroder, M. *Proc. Natl. Acad. Sci. U. S. A.* **2005**, *102*, 18280-18285

24) Ohki, Y.; Yasumura, K.; Kuge, K.; Tanino, S.; Ando, M.; Li, Z.; Tatsumi, K. *Proc. Natl. Acad. Sci. U. S. A.* **2008**, *105*, 7652-7657

25) Sellmann, D.; Lauderbach, F.; Heinemann, F. W. *Eur. J. Inorg. Chem.* **2005**, *2*, 371-377

26) Ohki, Y.; Sakamoto, M.; Tatsumi, K. *J. Am. Chem. Soc.*¸**2008**, *130*, 11610-11611

27) Ogo, S. *Chem. Comm*. **2009**, *23*, 3317-3325

28) Raugei, S.; Chen, S.; Ho, M.; Ginovska-Pangovska, B.; Rousseau, R. J.; Dupuis, M.; Dubois, D. L.; Bullock, R. M. *Chem. Eur. J.* **2012**, *18*, 6493-6506

29) DuBois, D. L.; DuBois, M. R. *Chem. Soc. Rev.*, **2009**, *38*, 62-72

30) Helm, M. L.; Stewart, M. P.; Bullock, R. M.; DuBois, M. R.; DuBois, D. L. *Science*, **2011**, *333*, 863-866

31) Ogo, S.; Matsumoto, T.; Kure, B. *Chem. Lett.* **2008**, *37*, 970-971

32) Ogo, S.; Ichikawa, K.; Kishima, T.; Matsumoto, T.; Nakai, H.; Kusaka, K.; Ohhara, T. *Science* **2013**, *339*, 682-684

33) Ogo, S.; Ichikawa, K.; Nonaka, K.; Matsumoto, T.; Kure, B.; Yoon, K.; Higuchi, Y.; Yagi, T. *Dalton Trans.* **2010**, *39*, 2993-2994

34) Rauchfuss, T. B. *Science*, **2007**, *316*, 553-554

Chapter 2

Ni-Superoxide Dismutase Structure and Function

2.1 Introduction

The structural characteristics of nickel superoxide dismutase (NiSOD) share some similarity with those of the DuBois mononuclear nickel H_2ase model as well as the Ogo heterobimetallic nickel-ruthenium model. Although NiSOD is a seemingly unrelated enzyme, it will be shown that metallopeptide-based mimics of NiSOD provide an ideal platform for Ni-coordination. Additionally the key structure function relationships within the NiSOD ligand set will be evaluated in an effort to determine which residues within the apopeptide must be conserved and which may be manipulated to allow the synthesis of a functional H_2ase mimic.

Superoxide dismutase (SOD) enzymes catalyze the disproportionation of superoxide into O_2 and hydrogen peroxide (H_2O_2), effectively reducing the oxidative stress resulting from aerobic cellular respiration.[1-9] Cellular damage caused by free radicals has been implicated in several diseases and disorders including inflammatory diseases, post-ischemic tissue injuries, Lou Gherig's Disease, Parkinson's Disease and has been connected to the aging process.[1,3,6] There are four classes of SOD which include CuZnSOD, MnSOD, FeSOD and the more recently discovered NiSOD, which has been found in *Streptomyces* and cyanobacteria. [1,3-5,6,8]

The two half-reactions by which SODs disproportionate superoxide are shown below (Eqn. 2.1-2.3). The metal center cycles between an oxidized and reduced state using superoxide as a reductant to form the relatively inert hydrogen peroxide and dioxygen species. The redox potential window for superoxide disproportionation lies between that of the O_2/O_2^- couple (-160 mV vs NHE) and the O_2^-/H_2O_2 couple (870 mV vs NHE) with an ideal value near 300 mV vs

NHE.[1,5,10] Interestingly, aqueous solutions of Cu, Mn and Fe have been found to disproportionate superoxide while aqueous nickel solutions display a redox potential well outside the SOD range and are incapable of SOD activity. This indicates significant influence of the protein framework on the redox activity of the NiSOD active site.[1,5,11] It is for this reason that the structure function relationships of coordinating residues will be examined in detail.

$$M^{ox} + O_2^- \longrightarrow M^{red} + O_2 \qquad \textbf{(eqn. 1)}$$

$$2H^+ + M^{red} + O_2^- \longrightarrow M^{ox} + H_2O_2 \qquad \textbf{(eqn. 2)}$$

$$\textbf{2H}^+ \textbf{+ O}_2^- \longrightarrow \textbf{H}_2\textbf{O}_2 \textbf{+ O}_2 \qquad \textbf{(eqn. 3)}$$

2.2 Nickel-based Superoxide Dismutase

The native NiSOD protein consists of a hexameric peptide assembly consisting of 117 peptidyl residues. Transportation of the superoxide substrate to the active site has been proposed to proceed through electrostatic interactions with positively charged lysine residues. These direct superoxide down the active site channel with a radius of approximately 3 Å which matches up nicely with the van der Waals radius of O_2^- (3.04Å).[1] Interestingly, the catalytic rate of disproportionation in the native enzyme was found to be pH-independent. This indicates that protons for H_2O_2 production do not come from solvent but instead from within the protein framework, suggesting an outer-sphere mechanism in which superoxide does not bind directly to the metal center.[12] The coordinated cysteine residues have been proposed to act as a proton source and a recent study by Shearer provides evidence for this.[2] Additional evidence for an outer-sphere mechanism was provided by Shearer and coworkers who demonstrated the inability of superoxide mimics such as azide ion and nitrosyl (NO^-) to bind to the Ni-center.[8] The

validity of an inner-sphere mechanism is still an issue of debate and will not be discussed further.[1,9]

The Ni-binding site of the protein is within the six N-terminal residues of the peptide chain and is referred to as the "Ni-hook" region due to the manner in which the peptide chain wraps itself around the metal center.[1] It is this region on which subsequent metallopeptides are synthesized. It has been observed that exposing NiSOD to cyanide strips the active site of Ni and that the Ni-hook region of the peptide becomes disordered, indicating a lack of pre-ordered entatic influence by the protein framework on the metal center.[1,13] The structural dependency of the active site on the presence of the nickel center is interesting because the ability of this enzyme to catalyze superoxide disproportionation is a sole consequence of the nature of the ligand set without the influence of a forced geometry. This suggests that a simplified approach to the development of functional models may be possible when compared to the geometrical and electronic hurdles of [NiFe]H_2ase models which are dictated by the protein environment rather than the presence of the Ni-center.

NiSOD facilitates superoxide disproportionation through a "ping-pong"-type mechanism in which the active site cycles between Ni(II) and Ni(III) oxidation states.[2,3,5,6,9] This is facilitated by the on/off ligation/dissociation of the N-terminal His(1) residue which binds to nickel through the δ-nitrogen atom of the imidazole ring and stabilizes the Ni(III) oxidation state.[1,3,9,11,14] The remainder of the Ni-hook coordination sphere consists of the N-terminal amine, a deprotonated amidate nitrogen from the peptide backbone and the Cys(2) and Cys(6) thiolates, all of which bind nickel in a square planar geometry with minimal distortion (Fig. 2.1).[1,5,9,11] The natural selection of this unique ligand set is quite interesting, as few metalloenzymes utilize a peptide backbone nitrogen and fewer still exhibit incorporation of the N-terminal nitrogen.[6] In addition,

coordinated thiolates are readily and often irreversibly oxidized, yet two are incorporated into a metalloenzyme which interacts exclusively and efficiently with oxygen and reactive oxygen species.[5,8,15,16] Many studies utilizing biological maquettes and biomimics have been conducted in order to elucidate the structure/function relationships of this unique ligand set which will be examined in order to select an appropriate ligand set for H_2 production.[5-9,15-19]

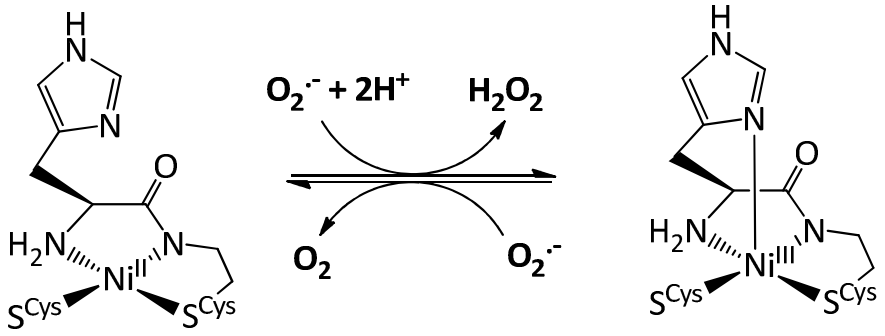

Figure 2.1 "Ping-pong" mechanism by which NiSOD disproportionates superoxide.[3]

2.3 NiSOD Structure and Function Relationships

In order to directly examine the nature of the native ligand set, Shearer and coworker produced a NiSOD maquette from the solid phase peptide synthesis of the first 12 N-terminal residues in the native enzyme.[3] The sequence, termed $NiSOD^{M1}$, coordinated Ni(II) in a 1:1 ratio and was found to exhibit spectroscopic, electrochemical and reactive properties representative of the native enzyme. The redox potential was initially measured at 0.70 V (vs Ag/Ag^+) using protein thin-film voltammetry on a carbon fiber ultramicroelectrode, but was revisited in a later study to gain more insight into the solution electrochemical properties of the active site.[4] This study instead used a standard three electrode cell (pyrolytic graphite edge working electrode, platinum-disk auxiliary electrode, SCE reference electrode) in a 1.0 mM solution of peptide (50 mM NEM buffer and a 100 mM NaCl supporting electrolyte) to yield a redox potential of 434 mV

(vs SCE), which is within 400 mV of the optimal value of 300mV vs. NHE.[4] This prompted investigation of the functionality of the maquette as an SOD. A *para*-nitro blue tetrazolium chloride (NBT)/formazan assay was subsequently performed in order to determine the maquette's ability to protect NBT from reduction upon addition of KO_2. It was found that up to 40,000 eq. of KO_2 could be added to a solution of $NiSOD^{M1}$ and NBT before the SOD became overwhelmed and the formation of formazan was observed confirming its catalytic functionality. Additionally, stopped-flow kinetics methods were performed as a more direct method for determining the catalytic activity of $NiSOD^{M1}$. The pseudo-first order rate constant for superoxide disproportionation by $NiSOD^{M1}$ (k_{cat} = 6.1 x 10^6 M^{-1} s^{-1}) was measured by monitoring the disappearance of O_2^- at 245 nm. [3,4] The ability of this maquette to mimic the native SOD enzyme provides a good starting place for the synthesis of a functional H_2ase-based metallopeptide mimic.

2.3.1 Axial Histidine Coordination

The main structural feature distinguishing the NiSOD active site from native [NiFe]H_2ase and its functional models is the presence of an axially coordinating histidine residue which allows formation of a square pyramidal geometry upon oxidation. The Shearer group has studied the structural, electronic and reactivity effects of axial coordination of the His(1) residue within the NiSOD ligand sphere. Using the shorter 7-residue $NiSOD^{M2}$ maquette, analogues of the active site were synthesized with substitution of the His(1) residue with alanine. This enabled a side-by-side comparison of the native imidazole-nitrogen coordination motif with a four-coordinate analogue to study the effects of omitting the axially coordinating imidazole ring from the active site. Electrochemical studies of the Ni^{2+}/Ni^{3+} couple showed an increase in redox potential from 0.52 V to 0.67 V vs Ag/Ag^+ upon replacement of His(1) with Ala as well as a

decreased peak to peak separation. Although there is a is shift in in redox potential from a four-coordinate to five-coordinate nickel center, both are within the SOD window. This indicates that coordination of an axial ligand stabilizes the Ni(III) center for reduction by superoxide but is not essential for redox activity.[5]

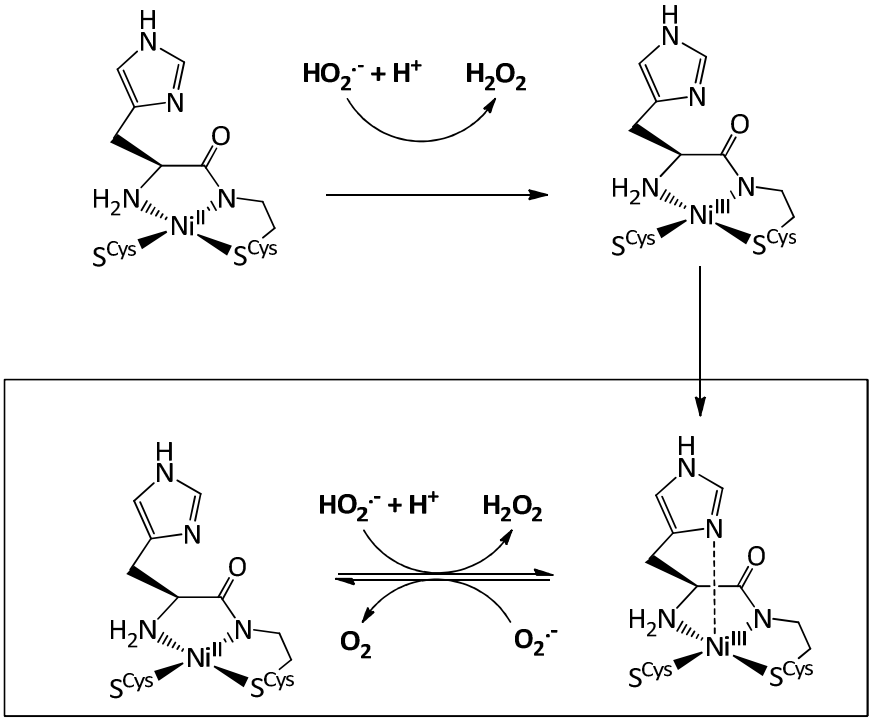

Figure 2.2 Proposed mechanism for initial ligation of the axial histidine followed by maintained coordination during catalytic disproportionation.[8]

A later study by the Shearer group considered the nature of the elongated Ni(III)-His bond distance (approx. 2.3 Å) in the crystal structure of the native enzyme when compared to typical Ni(III)-nitrogen bonds which are closer to 2.0 Å.[1,4] This elongation suggests that the protein manifold may hold the histidine residue at a distance as a means to optimize the active site.[9] In order to probe this structural feature the Shearer group manipulated the NiSOD^{M1} maquette to incorporate histidine residues of variable electron donating ability (Fig. 2.3). It was

proposed that providing the nickel center with a less Lewis basic axial nitrogen would increase the Ni-S bond strength and effectively contribute to the overall stability of the Ni(III) oxidation state.

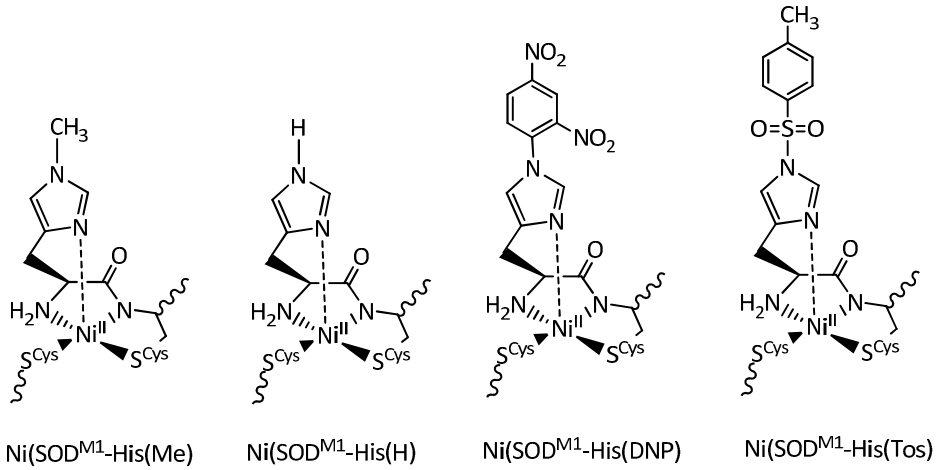

Figure 2.3 Modfied NiSOD^{M1}-H(1)-X maquttes (X = Me, H, DNP, Im-Tos) of variable electron donating/withdrawing ability for investigation of the influence of Lewis basicity (relative to the nickel center) on SOD reactivity.[4]

Electrochemical and reactivity studies were carried out to quantify the influence of Lewis basicity of the histidine ligand on catalysis. It was found that the redox potential of the Ni^{2+}/Ni^{3+} couple (vs Ag/Ag^{+}) increased as Lewis basicity was decreased. A measure of the rate of O_2^{-} disproportionation was performed using stopped flow kinetics and indicated a diminished k_{cat} as the Lewis acidity of the imidazole ring was increased. The rate for NiSOD^{M1}-(H), which contains an unmodified His residue, was found to be over an order of magnitude lower (7×10^7 $M^{-1}s^{-1}$) than that of the native enzyme (1×10^9 $M^{-1}s^{-1}$) while the less Lewis basic analogues showed greater activity toward superoxide disproportionation (4×10^8 $M^{-1}s^{-1}$ and 6×10^8 $M^{-1}s^{-1}$, respectively). When compared to the native enzyme it is evident that an entatic influence pulls the coordinating imidazole further from the nickel center in order to decrease the Lewis basicity

of the imidazole ring. This likely occurs through a H-bonding network between the imidazole ring and the nearby Glu(17) and Arg(47) residues.[4]

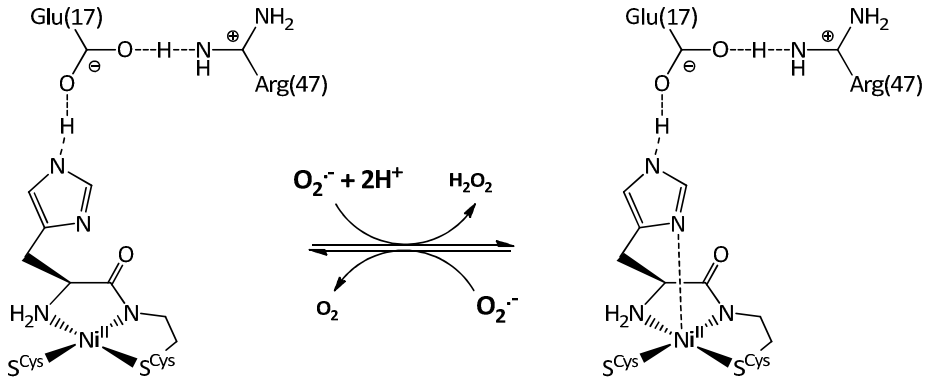

Figure 2.4 Proposed entatic influence of the protein framework on the Lewis basicity of the His(δ-N).[17]

2.3.2 *cis*-Cys Coordination

Nickel-cysteine coordination is observed in several other nickel-ligated metalloenzymes including Acetyl Coenzyme A Synthase, CO-dehydrogenase, Methyl Coenzyme M-Reductase as well as [NiFe] Hydrogenase. A study by Maroney and coworkers utilized Cys(2/6)Ser mutations to probe the structure/function relationship of the coordinating thiolates to the active site.[5] It was found through UV-Vis experiments that substitution of either cysteine residue resulted in the inability of any thiolate coordination to take place. This was evidenced by the disappearance of characteristic Cys-S → Ni charge transfer bands at 372nm. EPR and variable-temperature circular dichroism (CD) experiments confirmed that mutation at either Cys or at both was found to induce a high-spin Ni(II) center which results in loss of catalytic activity toward superoxide disproportionation. This suggests that bis-thiolate coordination is required for a catalytically active low-spin nickel center and stabilizes the Ni^{3+}/Ni^{2+} redox couple.[5,8,9]

There is also evidence that one or both cysteines may be involved in proton transfer to the superoxide substrate to form H_2O_2.[5,9] One such study conducted by Shearer evidences a proton-coupled electron-transfer event (PCET) upon reduction of Ni(III) to Ni(II).[2] The BDFE for $Ni(II)^{M1}$ -H, the protonated [$Ni^{II}(SOD^{M1})$] maquette, was determined using a modified Bordwell equation. This incorporated the $Ni(II)^{M1}$-H pKa (8.2) derived from differences in ligand field bands of $Ni(II)^{M1}$-H/$Ni(II)^{M1}$ as a function of pH as well as the [$Ni(SOD^{M1})$] redox potential (440 mV vs NHE). The resulting BDFE was found to be 79 kcal mol^{-1}, which is slightly less than the H-O BDFE for deprotonated H_2O_2 (81.6 kcal mol^{-1}), making reduction of the substrate through a PCET event thermodynamically favorable.

The next question addressed in this study was the location of the protonation site, which was determined from the X-ray absorption experiments obtained at pH 7.4 and 9.5.[4] The extended X-ray absorption fine-structure (EXAFS) spectrum, which allows determination of inter-atom distances within 0.1 pm, displayed a contraction in the Cys S-Ni(II) bond lengths from 2.20 Å to 2.18 Å upon decreasing the pH. This is suggestive of a thiolate protonation event and can be rationalized by considering the reduction in filled-filled Ni(π)/S(π) interaction upon protonation of the thiolate, leading to bond contraction.[2,9] Further inspection of the native NiSOD crystal structure shows a shorter Cys6 S-Ni bond length than that of Cys2 S-Ni, implicating the the Cys6 thiolate as the protonation site. The S K-edge spectrum of the $Ni(III)SOD^{M1}$ taken at pH 7.4 indicates deprotonation of a thiolate moiety upon oxidation, leading to the proposition that the PCET event takes place upon reduction/protonation of superoxide and concomitant oxidation of the nickel center (Fig. 2.5). These data strongly suggest the NiSOD metallopeptide contains an internal base capable of facilitating PCET reactions.[2]

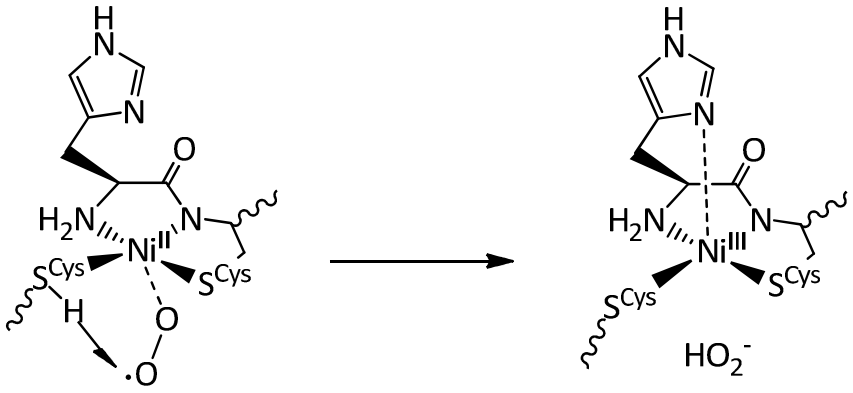

Figure 2.5 Proton transfer from protonated Cys(6) thiolate moiety to superoxide.[2]

2.3.3 Mixed Amine/Amidate Coordination

Previous spectroscopic and computational studies by the Brunold and Grapperhaus groups on variable amine/amidate ligation motifs describe the functionality of the unique mixed ligand set as a shield against oxidative damage of the cysteine sulfurs.[9,19,20] Bisamidate ligation was found to protect coordinated thiols by lowering the amount of sulfur character in the redox-active molecular orbital to effectively stabilize the Ni^{3+} oxidation state and promote a Ni-centered oxidation.[9] It was also suggested that the Ni/S HOMO is susceptible to nucleophilic attack and that replacement of anionic N-donors with neutral amines decreases the energy of the HOMO, effectively lowering reactivity toward reactive oxygen species (ROS).[6,17,19,20] Both of these perspectives were considered concomitantly in a study of model compounds of variable amine/amidate ligation by Shearer et al in which the electronic structure of the bisamine compound (bmmp-dmed)Ni^{II}, the mixed amine/amidate compound $(Ni^{II}(BEAAM))^-$ and the bisamidate compound $(Ni^{II}(emi))^{2-}$ were probed using Ni L-edge and S K-edge XAS in tandem with electronic absorption experiments and ab initio calculations (Fig. 2.6).[17]

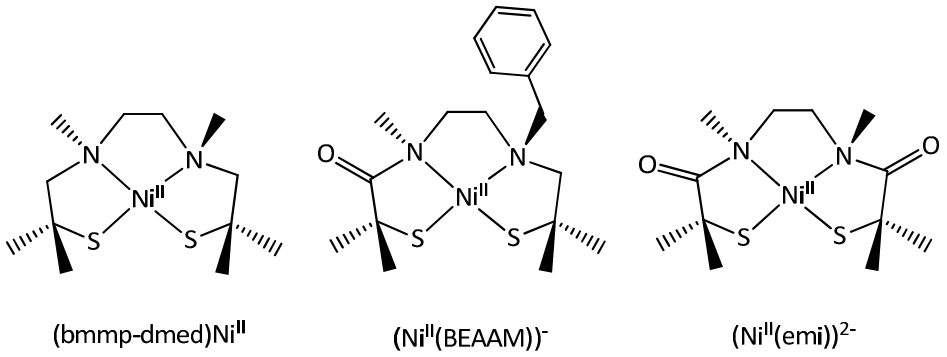

Figure 2.6 Model Ni^{II}SOD mimics of variable amine/amidate ligation.[17]

The results of this study can be summarized via the crystal field-splitting energy diagrams (Fig. 2.7) which illustrate the degree of S-character and Ni-character in the redox-active molecular orbital (RAMO) as well as the energy of the HOMO. From this several trends can be observed. The first is that decreased amidate ligation to the metal center results in a lower Ni(3d) energy and a subsequent decrease in covalency of the HOMO, which is consistent with studies by Grapperhaus.[19,20] Additionally it can be observed that replacement of a single amine in the bisamine complex to give the mixed amine/amidate results in a better Ni(3d)-S(π)/S(π)* matchup and a more covalent HOMO. Increasing the anionic character of the ligand set further to afford the bisamidate complex decreases the overall S-character in the RAMO greatly while destabilizing the Ni(3d) orbital to a higher energy higher than that of S(π)/S(π)*. This affords a much more stable Ni^{3+} center with less chance of sulfur-based oxidation owing to the high degree of Ni-character, however this also results in a relatively high energy and highly nucleophilic HOMO.[16] These observations are in line with the conclusions drawn by Brunold.[9]

The second trend can be observed from the experimental one-electron oxidations of $(Ni^{II}(BEAAM))^-$ and $(Ni^{II}(emi))^{2-}$, which are both reversible, while (bmmp-dmed)Ni^{II} undergoes irreversible oxidative modification.[9,16,20] Additionally (bmmp-dmed)Ni^{II} and $(Ni^{II}(BEAAM))^-$ were

found to be stable in air for extended periods of time while $(Ni^{II}(emi))^{2-}$ undergoes rapid oxygenation.[9,15,16] The big picture here is that while a bisamine coordination motif results in decreased covalency of the HOMO, the large degree of S-character in the RAMO leaves it susceptible to sulfur-based oxidation. Additionally the bisamidate coordination motif forces a Ni-based oxidation, however the resulting highly covalent Ni(3d)- S(π)/S(π)* based HOMO promotes electrophilic attack by O_2 and ROS. It thus becomes evident that the mixed amine/amidate coordination motif is essential to minimizing susceptibility of the HOMO to electrophilic attack while promoting Ni-based oxidation during turnover.

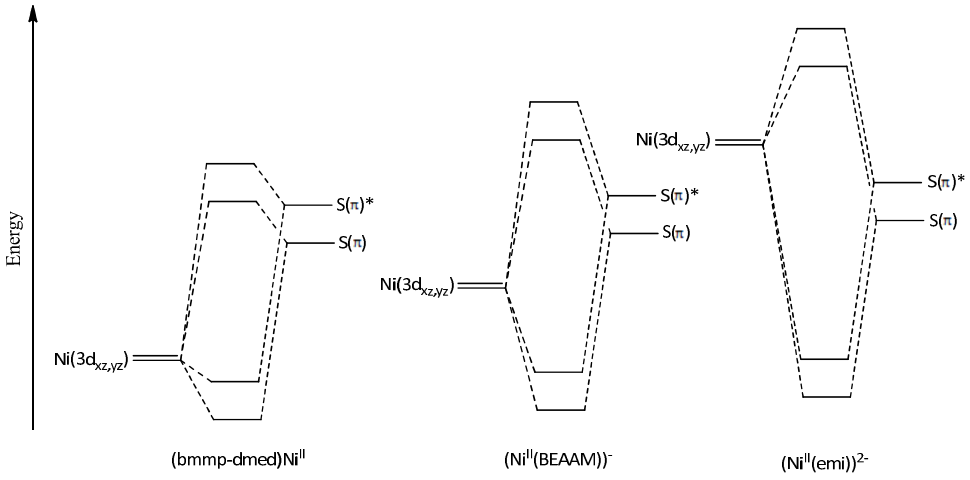

Figure 2.7 Crystal field splitting diagrams generated from hybrid-DFT and SORCI calculations for (bmmp-dmed)Ni^{II}, $(Ni^{II}(BEAAM))^{-}$ and $(Ni^{II}(emi))^{2-}$ (left to right).[17]

During initial studies of the $NiSOD^{M1}$ maquette by Shearer and coworker the electrochemistry and reactivity of $[Ni^{II}(emi)]^{2-}$ and the bisamidate mimic $[Ni^{II}(bmedach)]$, were also inspected.[3] The intent was to probe the structure/function relationship of the unique N-terminal amine/peptide amidate ligand set by comparison to compounds with bisamine and bisamidate coordination motifs. In order to investigate these findings experimentally, a *para*-

nitro blue tetrazolium chloride (NBT)/formazan assay of the two model complexes was performed to quantify their ability to disproportionate superoxide upon exposure to KO_2. The inability of both compounds to protect NBT from reduction by superoxide was rationalized by examining their respective redox potentials. The bis-amine motif afforded a positively shifted Ni^{2+}/Ni^{3+} redox potential ($E_{1/2}$ > 1.2 V vs Ag/Ag^{+}) which is outside of the SOD window for superoxide reduction while the bis-amidate motif had a negatively shifted redox potential ($E_{1/2}$ = -0.40 V vs Ag/Ag^{+}) that prevents it from oxidizing superoxide to regenerate the Ni(II) oxidation state. This suggests that in addition to providing oxidative protection of the active site, an amine/amidate motif plays a significant role in fine tuning the nickel center for optimized electrochemical performance within the SOD window.[3]

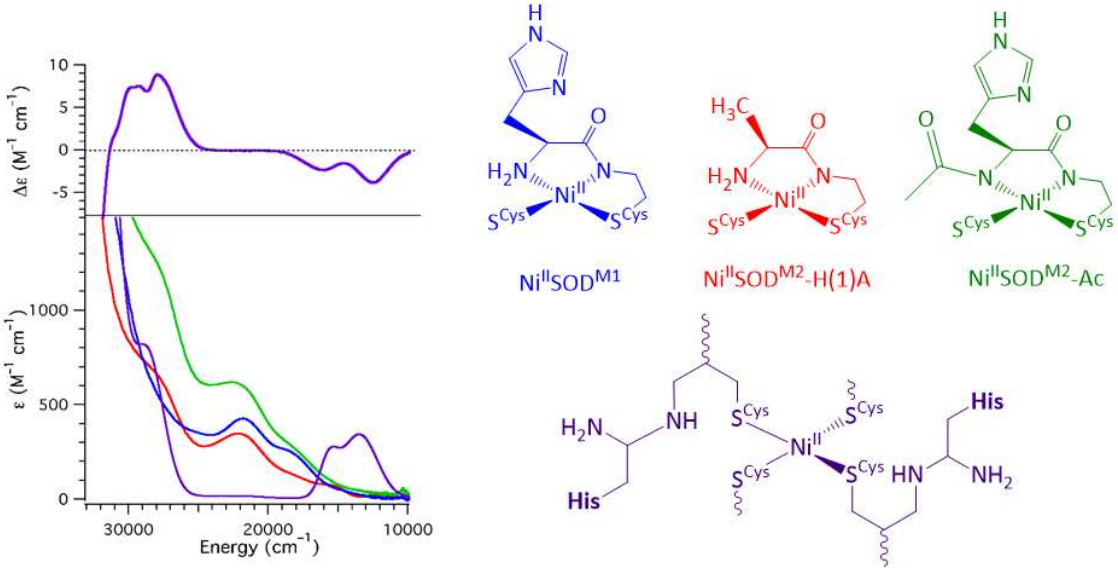

Figure 2.8 The CD spectrum of $Ni(Cys2/6)_2$ tetrahedral metallopeptide (top left) lacking available amidate coordination to the nickel center. This results in a 2:1 peptide to nickel binding motif (purple trace). UV-Vis spectrum (bottom) $NiSOD^{M1}$-Ac (green trace), $NiSOD^{M1}$ (blue trace), $NiSOD^{M1}$-H(1)A (red trace).[21]

The importance of amidate coordination may also extend into the ability of the "Ni-hook" segment of the SOD peptide to ligate Ni. Unpublished EXAFS data put forth by Shearer (**Fig. 8**) suggests the backbone amidate nitrogen is central in anchoring the nickel center to the peptide. The UV-Vis and CD data (Fig. 2.8) shows a decreasing extinction coefficient resulting from decreased Ni-S covalency as amidate ligation is decreased from $NiSOD^{M1}$-Ac (green) motif to the mixed amine/amidate species $NiSOD^{M1}$ (blue) and $NiSOD^{M1}$-H(1)A. Upon removal of amidate moieties from the Ni-hook region of the apopeptide it is apparent that nickel does not coordinate in a square planar environment as is evidenced by the purple trace in the UV-Vis spectrum. The CD spectrum (top) suggests the formation of a tetrahedral NiS_4 complex and can be explained by a 2:1 binding mode of peptide to nickel through the Cys2 and Cys6 residues and the absence of nitrogen coordination. This indicates that the presence of an amidate moiety within the coordination sphere is essential for the formation of mixed S/N ligation to nickel in a 1:1 ratio.[21]

2.4 Summary

All of these studies have shown that the *N*-terminal amine and amidate nitrogens play a significant role in dictating the coordination geometry and electronics of the NiSOD active site. Additionally, the presence of an amidate nitrogen is essential for coordination of Ni(II) to the apopeptide and cysteine-thiolates have been implicated in the transfer of protons upon reduction of the Ni(II) center of the metallopeptide. The role of the axially coordinating histidine residue was found to be unnecessary for the coordination of nickel to the apopeptide and its removal is proposed to impose minimal disruption to the stability of the remaining ligands. The incorporation of thiolate moieties allows transfer of protons within the active site

upon oxidation of the metal center has suggested that coordinated cysteine residues have the potential to function as internal bases for the formation of nickel hydride intermediates for H_2 production.

2.5 References

1) Getzoff, E. D.; Barondeau, D. P.; Kassmann, C. J.; Bruns, C. K.; Tainer, J. A. *Biochemistry*, **2004**, *43*, 8038-8047

2) Shearer, J.; *Angew. Chem. Int. Ed.*, **2013**, *52*, 2569-2572

3) Shearer, J.; Long, L. M. *Inorg. Chem.* **2006**, *45*, 2358-2360

4) Shearer, J.; Neupane, K. P.; Callan, P. E. *Inorg. Chem.*, **2009**, *48*, 10560-10571

5) Maroney, M. J.; Ryan, K. C.; Johnson, O. E.; Cabelli, D. E.; Brunold, T. C. *J. Biol. Inorg. Chem.*, **2010**, *15*, 795-807

6) Shearer, J.; Neupane, K. P. *Inorg. Chem.* **2006**, *45*, 10552-10566

7) Shearer, J. *J. Inorg. Biochem.*, **2013**, *129*, 145-155

8) Shearer, J.; Neupane, K. P.; Gearty, K.; Francis, A. *J. Am. Chem. Soc.* **2007**, *129*, 14605-14618

9) Brunold, T. C.; Fiedler, A. T.; Bryngelson, P. A.; Maroney, M. J. *J. Am. Chem. Soc.* **2005**, *127*, 5449-5462

10) Maroney, M. J.; Herbst, R. W.; Guce, A.; Bryngelson, P. A.; Higgins, K. A.; Ryan, K. C.; Cabelli, D. E.; Garman, S. C. *Biochemistry*, **2009**, *48*, 3354-3369

11) Maroney, M. J.; Bryngelson, P. A.; Arobo, S. E.; Pinkham, J. L.; Cabelli, D. E. *JACS*, **2004**, *126*, 460-461

12) Maroney M. J.; Choudhury S. B.; Lee J. W.; Davidson G.; Yim Y; Bose K.; Sharma M. L.; Kang S. O.; Cabelli D. E. *Biochemistry* **1999**, *38* 3744-3752

13) Williams, J. P.; Vallee, B. L. *Proc. Natl. Acad. Sci.* **1968**, *59*, 498-505

14) Holm, R. H.; Kruger, H. J.; Peng, G. *Inorg. Chem.* **1991**, *30*, 734-742

15) Shearer, J.; Zhao, N. *Inorg. Chem.* **2006**, *45*, 9637-9639

16) Hegg, E. L.; Shearer, J.; Mathrubootham, V.; Thomas, J.; Stables, R.; McCraken, J. *Inorg. Chem.* **2010**, *49*, 5393-5406

17) Shearer, J.; Dehestanl, A.; Abanda, F. *Inorg. Chem.* **2008**, *47*, 2649-2660

18) (a) Harrop, T. C.; Gale, E. M.; Simmonett, A. C.; Tesler, J.; Shaefer, III, H. F. *Inorg. Chem.* **2011**, *50*, 9216-9218
(b) Harrop, T. C.; Gale, E. M.; Patra, A. K. *Inorg. Chem.* **2009**, *48*, 5620-5622
(c) Harrop, T. C.; Gale, E. M.; Narendrapurapu, B. S.; Simmonet, A. C.; Schaefer III, H. F. *Inorg. Chem.* **2010**, *49*, 7080-7096
(d) Harrop, T. C.; Gale, E. M.; Cowart, D. M.; Scott, R. A. *Inorg. Chem.* **2011**, *50*, 10460-10471

19) Grapperhaus, C. A.; Mullins, C. S.; Kozlowski, P. M. *J. Biol. Inorg. Chem.* **2006**, *11*, 617-625

20) Grapperhaus, C. A.; Mullins, C. S.; Kozlowski, P. M.; Mashuta, M. S. *Inorg. Chem.* **2004**, *43*, 2859-2866

21) Shearer, J.; Unpublished Data

Chapter 3

Incorporation of a Phosphine into the NiSOD Coordination Environment to Afford a Hydrogenase Model

3.1 Functionalizing the NiSOD Ligand Set for H_2 Production

Upon evaluation of the structure function relationships observed in NiSOD metallopeptides, it was determined that removal of the axially-coordinating histidine moiety will result in minimal modification to the stability and geometry of the active site. We will exploit the inherent stability these ligands provide by altering the *N*-terminal amine residue to an isoelectronic softer phosphine residue. It is reasonable that such a modification will allow us to retain many of the properties inherent to NiSOD, including an amidate functionality for anchoring Ni(II) to the peptide and thiolate functionalities for the shuttling of protons from solvent to the nickel center. Specifically, it is proposed that incorporation of a phosphine at the *N*-terminal site with enforce a NiL_4 coordination motif and stabilize lower Ni oxidation states without disrupting the ability of the active site to form hydride complexes.

3.2 Incorporation of 1,3,5-triaza-7-phosphatricyclo[3.3.1.1]decane (PTA)

1,3,5-triaza-7-phosphatricyclo[3.3.1.1]decane (PTA) is an air-stable and water soluble phosphine ligand and has been used previously in organometallic chemistry and catalysis.[1] Tertiary amine nitrogens in the lower rim of the PTA architecture allow multiple sites for hydrogen bonding and subsequent high solubility in polar solvents. The structure and electronics of PTA have been likened to that of trimethylphosphine (PMe_3) owing to its low stearic demand and strong binding to metal centers with the added advantages of stability in air and solubility in polar environments.[2]

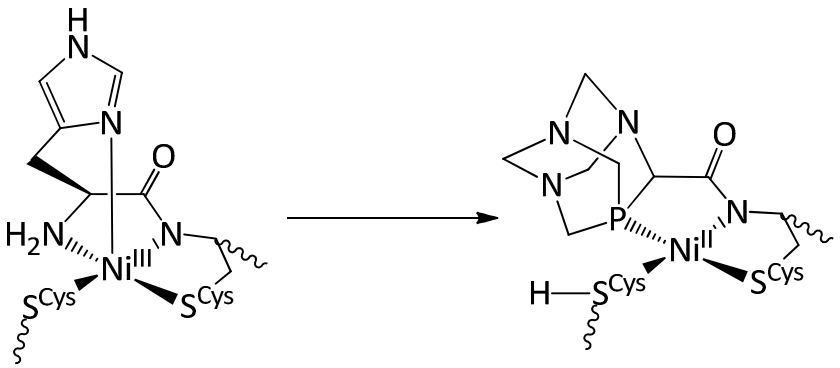

Figure 3.1 Substitution of His(1) in NiSOD for a PTA ligand to afford {$Ni^{II}(H_2ase^{M2})$} as a potential H_2ase mimic.

The incorporation of PTA as a ligand into the NiSOD binding motif is attractive for several reasons. First, it is a neutral two electron Lewis base, making substitution of the *N*-terminal amine a feasible option without significant disruption of the structure and electronics of the native coordination environment. This can be accomplished by chemical modification of an upper rim carbon α to the phosphorus atom to incorporate a carboxyl functionality (Fig. 3.2).[3] This allows ease of addition to the apopeptide using standard solid-phase peptide synthesis procedures.

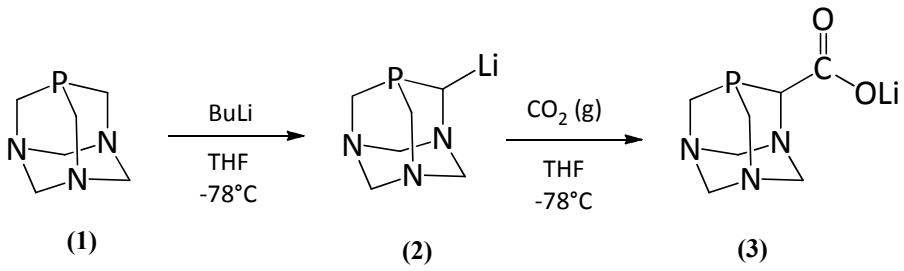

Figure 3.2 Upper-rim modification of PTA to afford a carboxylate moiety (PTA-COOLi).[3]

The increased σ-donor and π-acceptor abilities of a phosphine ligand may have some inherent advantages as well. When comparing mixed amine/amidate ligation to a bisamidate

motif, higher σ-bonding interactions between amide nitrogens and the metal center are observed. This is manifested in higher energy transitions in the UV-Vis spectrum for the bisamide complex and is supported by electronic structure calculations.[4] The resulting increased HOMO destabilization and an increased LUMO energy has been demonstrated to provide protection of coordinated thiols against one-electron oxidative damage at the expense of increased susceptibility to electrophilic attack of the thiols by reactive oxygen species (ROS).[4-6] The π-accepting ability of PTA has the added advantage of reducing filled-filled Ni(π)/S(π) interaction of the sulfur *trans*- to it, subsequently shortening the Ni-S bond length and decreasing the likelihood of a sulfur-based one-electron oxidation. The disadvantage of this π-back donation is the subsequent activation of the RAMO toward electrophilic attack by reactive oxygen species (ROS).

Because the native NiSOD active site lacks any entatic influence on the geometry about the nickel center, the ligand set is observed to be square planar with minimal distortion.[6-9] The incorporation of moderately bulky ligand such as PTA (Tollman cone angle ~ 103°) may provide tetrahedral distortion to some degree without inhibiting the binding of the Cys(6) thiolate.[10] Distortion at the metal center is a common feature of both the native [NiFe]H_2ase and DuBois' mononuclear model H_2ase.[11,12] Another common feature of [NiFe]H_2ase models involves the use of an internal base acting as a proton relay between solution and the metal center allowing guided proton transfer in close proximity with the metal.[13-16] The role of the coordinated thiolate moieties in proton transfer within the NiSOD coordination sphere, therefore, necessitates conservation of the bis-Cys motif.[13,14,17]

In summary, replacement of the *N*-terminal histidine and amine functionalities with a chelating phosphine thereby opens up the NiSOD active site to function as a potential H_2ase.

Additionally, conservation of the coordinated amide and bis-cysteine thiol functionalities are essential in stabilizing a variety of oxidation states and facilitating catalytic proton transfer to the metal while remaining robust to redox processes. A conceptual mechanism for the production of H_2 using the {$Ni^{II}(H_2ase^{M1})$} maquette is shown in Fig. 3.3.

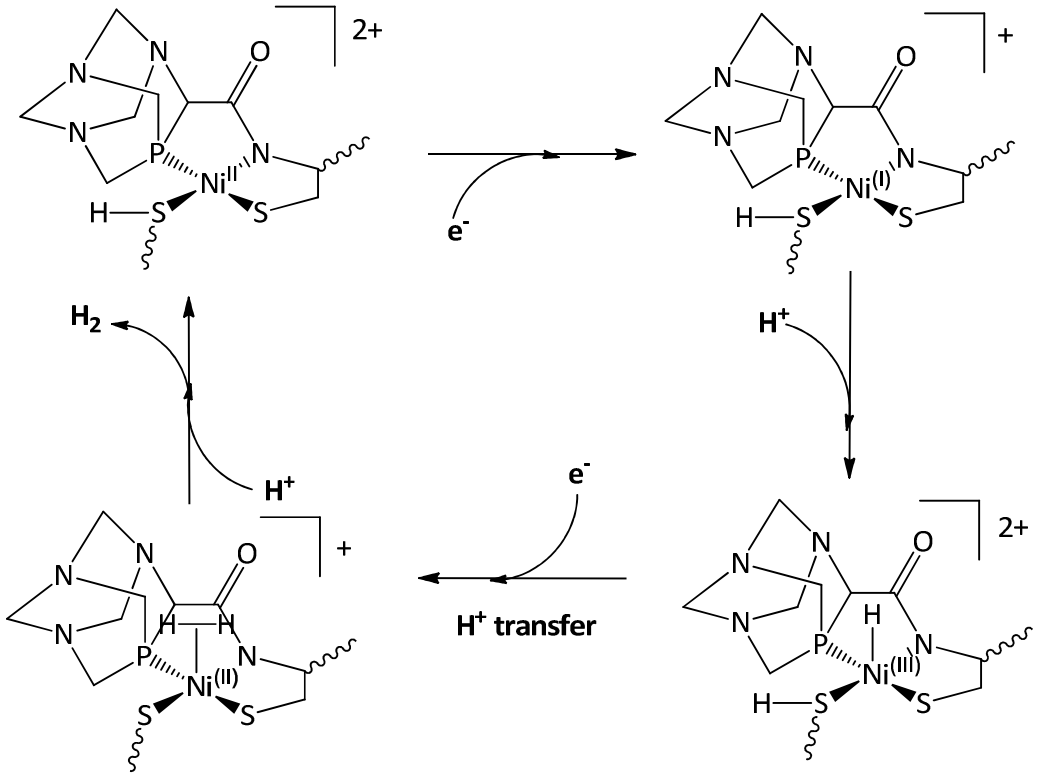

Figure 3.3 Conceptual mechanism for H_2 production by {$Ni^{II}(H_2ase^{M1})$}.

3.3 Grafting {[Ni]H_2ase} Metallopeptide to a Functionalized Electrode

In order to gain insight into the feasibility of this mechanism as well as the stability of the {$Ni^{II}(H_2ase^{M2})$} active site electrochemical experiments must be performed. This can be accomplished by covalently grafting the peptide to a functionalized working electrode to simulate electron transfer pathways within the native enzyme and potentially prolong the life of the peptide by avoiding conditions that may rapidly denature the enzyme. Baffert and

coworkers recently described a method by which [FeFe] hydrogenases were covalently grafted to pyrolytic graphite electrodes through a peptide coupling process.[18] This was accomplished first by coating the electrode in 4-carboxybenzenediazonium or nitrobenzenediazonium, the latter of which requires reduction in the presence of acid to afford the aniline functionality. This was followed by addition of coupling reagents *N*-hydroxysuccinimide (NHS) and 1-ethyl-3-(3-dimethylaminopropyll) carbodiimide (EDC) to the electrode surface and subsequent "painting" on of a dilute solution containing the H_2ase. Coupling between carboxyl and amine groups on the functionalized electrode surface and the H_2ase effectively tethered the enzyme directly to the electrode for electrochemical study.

Application of this methodology into the study of the $\{Ni^{II}(H_2ase^{M2})\}$ catalyst requires proper functionalization of the peptide *C*-terminus to allow coupling to the electrode. This can be done simply by incorporating an additional aspartic acid or lysine residue to the *C*-terminus during peptide synthesis. These two residues were chosen based on their respective amine and carboxyl functionalized R-groups which should allow relatively straightforward coupling to carboxybenzene- or aniline-functionalized surfaces. Subsequent investigation of the electrochemical properties of $\{Ni^{II}(H_2ase^{M2})\}$ and analysis of the headspace for H_2 production will give insight into its ability to function as a catalytic H_2ase model.

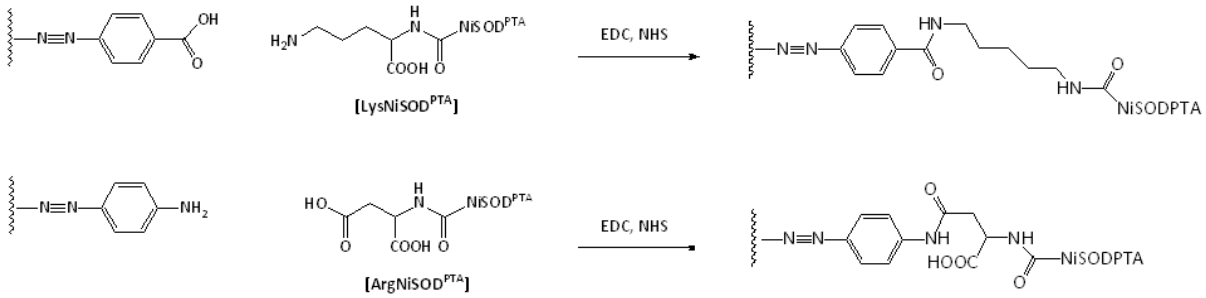

Figure 3.4 Coupling of {$Ni^{II}(H_2ase^{M2}$-Lys)} (top) and {$Ni^{II}(H_2ase^{M2}$-Asp)} (bottom) to a functionalized electrode.[18]

3.4 Results and Discussion

Successful synthesis and coupling of PTA-COOLi to the $H_2ase^{M1/2}$ apopeptide was confirmed through $^{1}H/^{31}$PNMR and HPLC experiments. Subsequent electronic absorption and X-ray absorption experiments were conducted to investigate the coordination environment upon nickel-coordination. A detailed description of methods and procedures is provided in Chapter 4.

3.4.1 Synthesis of Lithium 1,3,5-Triaza-7-phosphaadamantane-6- carboxylate (PTA-COOLi)

Characterization of PTA-carboxylate by nuclear magnetic resonance yields chemical shifts consistent with previously reported values with the exception of a large residual D_2O peak (4.65 ppm).[3] The ^{1}HNMR spectrum (D_2O, 500 MHz) features a multiplet with chemical shifts ranging from 4.50-4.21 ppm corresponding to lower-rim protons (NC*H*$_2$N) as well as multiplet centered at 3.90, which corresponds to the proton bound to the stereogenic carbon (PC*H*N), and a multiplet at 3.75-3.63 ppm corresponding to the other upper-rim protons bound to unmodified carbons (PC*H*$_2$N). The ^{31}PNMR (D_2O; referenced to 85% H_3PO_4 in D_2O) spectrum displays a weak singlet at -90.1 ppm.

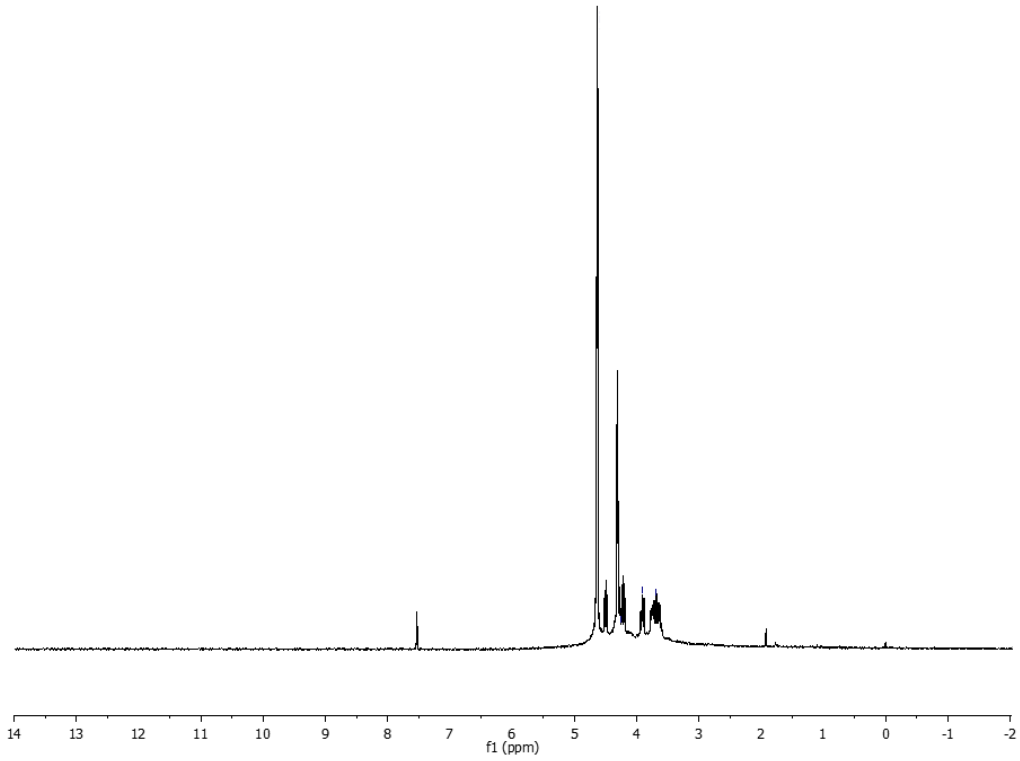

Figure 3.5 Full ^{1}HNMR spectrum for PTA-COOLi (D_2O).

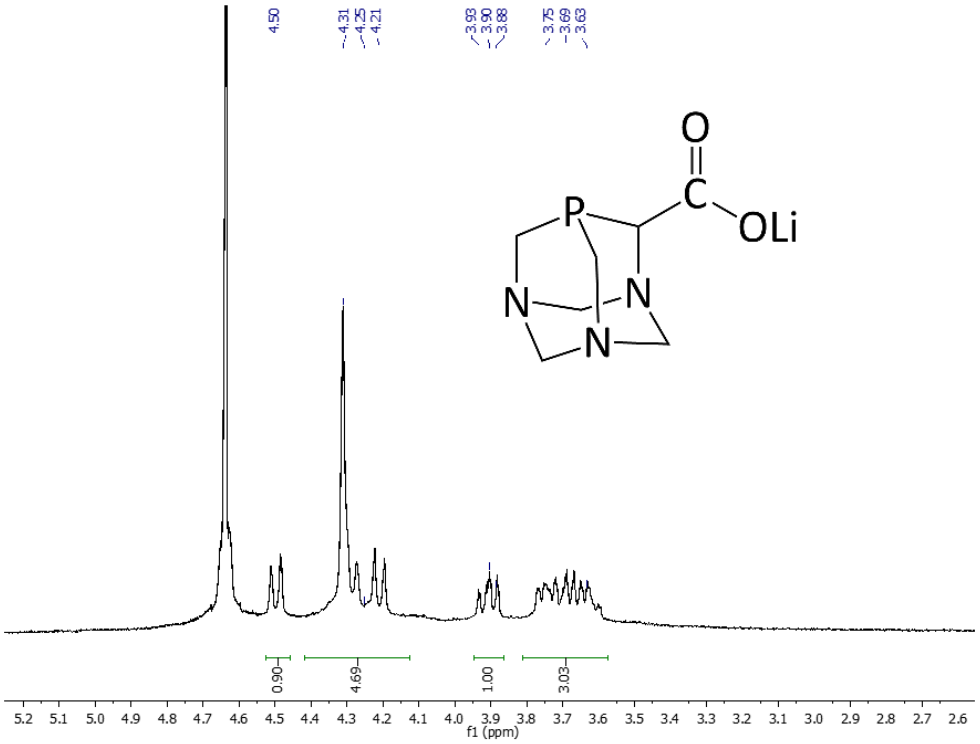

Figure 3.6 ^{1}HNMR spectrum for PTA-COOLi (D_2O) enlarged to observe peaks of interest.

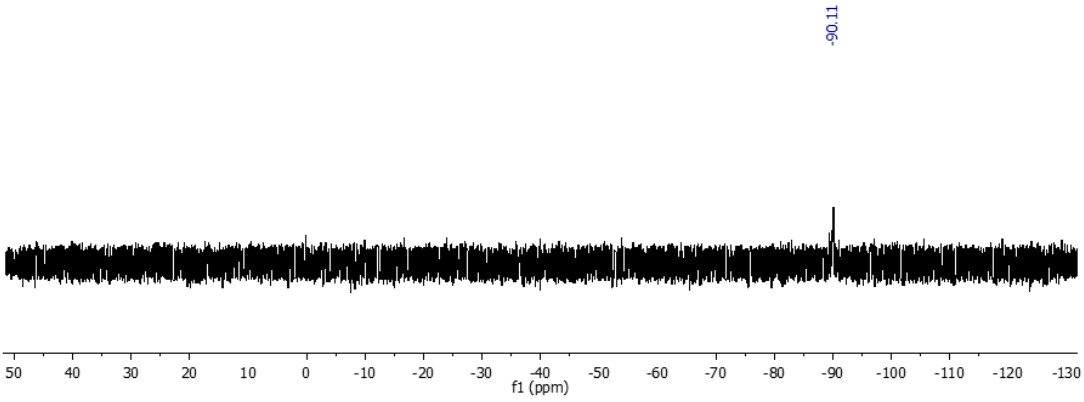

Figure 3.7 ^{31}PNMR spectrum for PTA-COOLi (D_2O).

3.4.2 Metallopeptide Synthesis

Coupling of the PTA-carboxylate residue to the apopeptide utilizing traditional SPPS coupling methods was complicated by the low solubility of PTA-COOLi in DMF (dimethylformamide) and NMP (*N*-methyl-2-pyrrolidone), both of which are solvents required for SPPS. It was found that coupling of PTA-COOLi required initial solvation in minimal DMSO (dimethyl sulfoxide) followed by addition of coupling reagents, minimal DMF and two to three drops of pyridine to increase the basicity of the solution. To quantify addition of the PTA functionality to the peptide ESI-MS (section 3.4.3) experiments were performed on the apopeptides ({H_2ase^{M2}-Asp} and {H_2ase^{M1}-Lys}) and subsequent ^{31}PNMR (section 3.4.4) was performed on the metallopeptide {$Ni^{II}(H_2ase^{M2}$-Asp)}.

3.4.3 HPLC and ESI-MS Experiments

Following peptide synthesis, all peptides were purified by reverse phase HPLC on a Waters DeltaPrep-600 utilizing a Waters X-Bridge C-18 column and their purity assed by analytical reverse-phase HPLC experiments (see section 4.4 for details). Below are the semi-prep and analytical chromatograms for the H_2ase^{M2}, H_2ase^{M2}-Asp and H_2ase^{M2}-Lys apopeptides which display similar retention times of 17.27, 17.99 and 18.09, respectively with peaks prior to five minutes corresponding to solvent. This indicates that modification of the *C*-terminus of the apopeptide results in minimal changes in the elution time of the $H_2ase^{M1(2)}$ peptide.

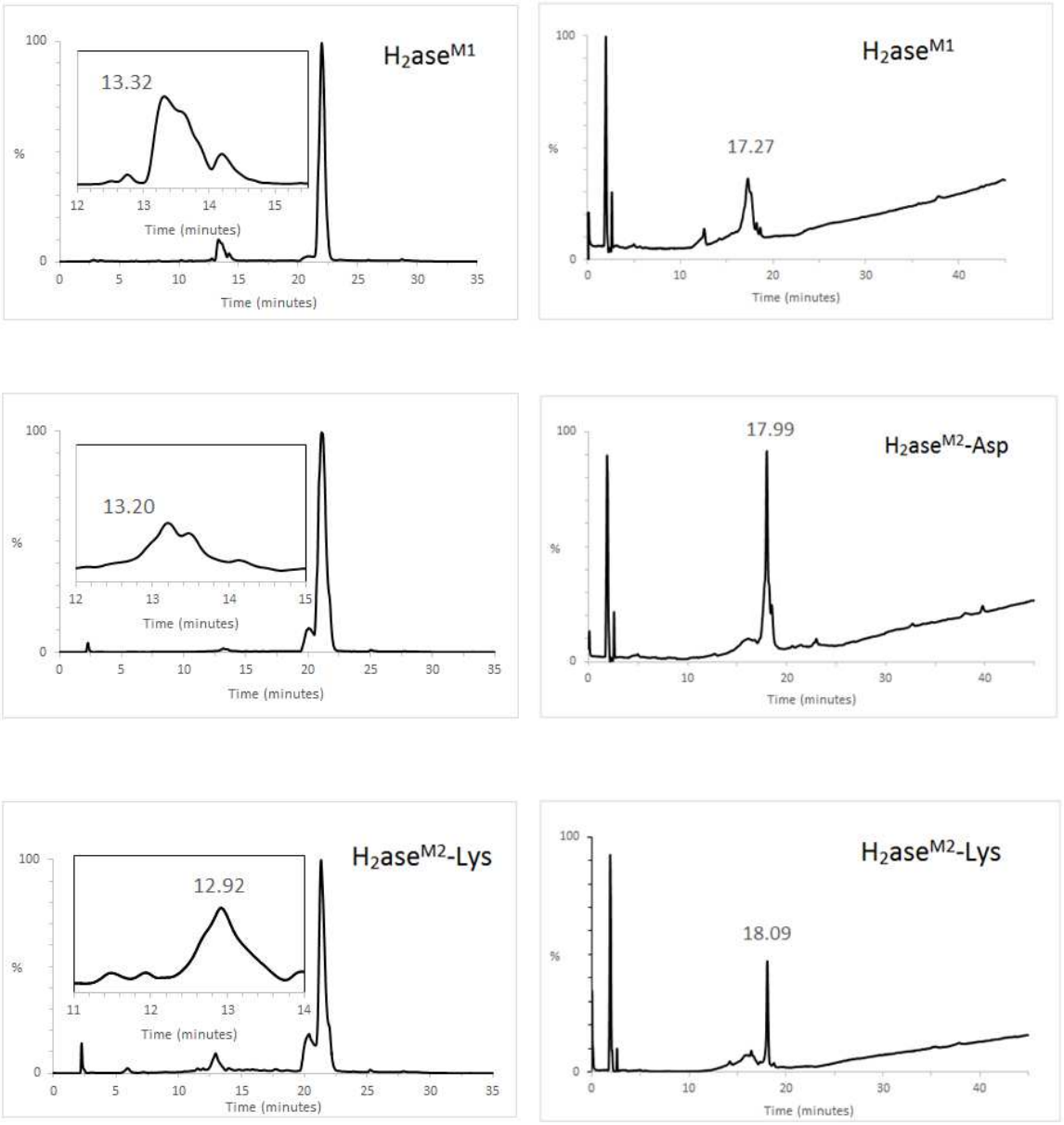

Figure 3.8 Retention times with insets depicting peaks collected for (H_2ase^{M1}, H_2ase^{M2}-Asp and H_2ase^{M2}-Lys) apopeptides after semiprep purification (left) and analytical (right) reverse phase HPLC on a Waters DeltaPrep 600 and Waters X-Bridge C-18 column.

Additional ESI-MS experiments were performed to analyze the purity of the {H_2ase^{M2}-Asp/Lys} peptides. Data for {H_2ase^{M2}-Asp} was collected at the Proteomics Center at the University of Nevada-Reno via direct-infusion LCMS. These spectra were inconclusive and a

subsequent ^{31}PNMR experiment was performed after metallation of the apopeptide to confirm coupling of the PTA functionality. Data for {H_2ase^{M2}-Lys} was collected on a Waters MicroMass 20 ESI mass spectrometer (positive ion mode) and seemed to indicate that the PTA functionality may not have successfully coupled to the peptide. The predicted *m/z* $(M)^+$ for {H_2ase^{M2}-Lys} is 1464.6 while scission of the peptide bond between PTA and the peptide predicts a *m/z* $(M)^+$ of 1279.5 and $(M+2)^+$ of 640.7 which is in better agreement with the observed peaks at 1274.7(5) and 638.5(7), respectively (Fig. 3.9).

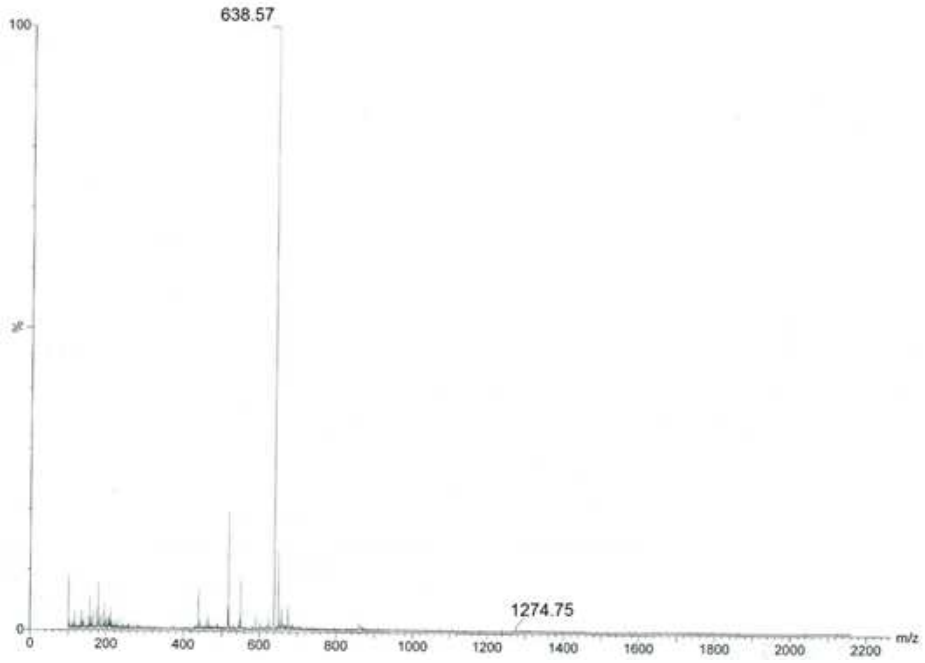

Figure 3.9 ESI-MS data for {H_2ase^{M2}-Lys}

3.4.4 Metallopeptide ^{31}PNMR Experiments

In an effort to supplement the HPLC and ESI-MS data, ^{31}PNMR spectroscopy proved to be a quick and direct method for confirming the presence of PTA within the metallopeptide after coordination to the nickel center. The presence of a single phosphorus atom within the {$Ni^{II}(H_2ase^{M2}$-Asp)} metallopeptide results in a weak single singlet peak at -43.33 ppm. This is

near the literature value for $Ni(PTA)_4$ at -46.5 ppm which is reported with several PTA-coordinated nickel complexes including $Ni(CN)_2(PTA)_3$, $Ni(CO)(PTA)_3$, $Ni(CO)_3(PTA)$, and $[Ni(NO)(PTA)_3]N$ with chemical shifts ranging from -46 to -54 ppm.[10] However, the chemical shift observed in this spectrum is unexpected as electronic absorption (section 3.4.4) and X-ray absorption (section 3.4.5) studies have suggested the presence of a high-spin Ni-center resulting from a distorted tetrahedral geometry, suggesting that one or more species may be present. Additionally, two peaks would be expected owing to the chirality of the phosphine prior to coordination.

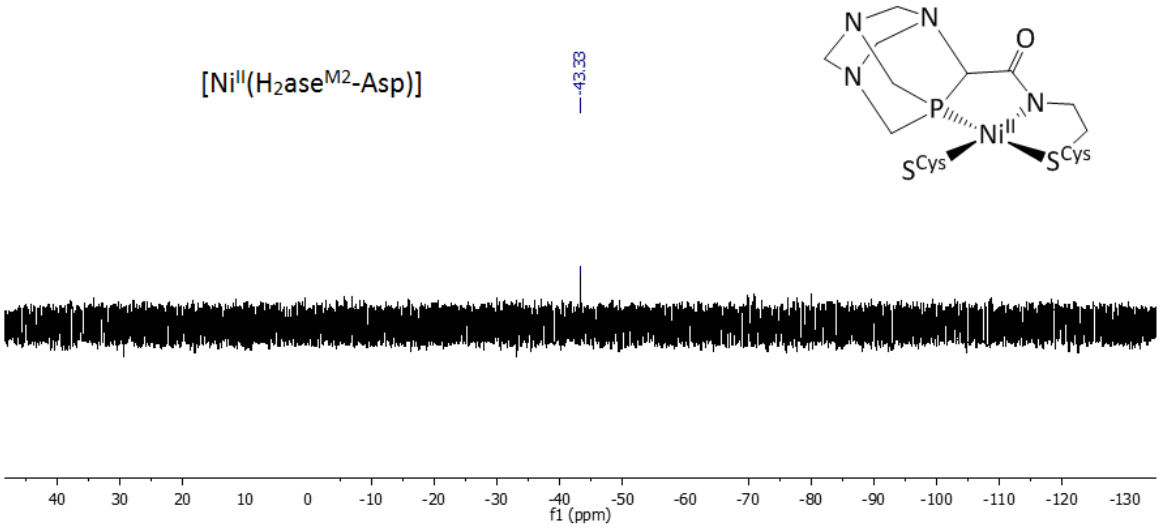

Figure 3.10 ^{31}PNMR spectrum of $\{Ni^{II}(H_2ase^{M2}\text{-Asp})\}$ metallopeptide (CD_3OD).

3.4.5 Electronic Absorption Studies of $\{Ni^{II}(H_2ase^{M2}\text{-Asp})\}$

The main features observed in the UV-Vis spectrum of $\{Ni^{II}(H_2ase^{M2}\text{-Asp})\}$ include a transition at 278 nm (5712 M^{-1} cm^{-1}) and a shoulder at 321 nm (2970 M^{-1} cm^{-1}) just before the onset of end absorbance. Additionally a broad transition at 385 nm (927M^{-1} cm^{-1}) as well as

features at 503 nm (239 M^{-1} cm^{-1}) and 541 nm (177 M^{-1} cm^{-1}), the last of which is also observed for $Ni^{II}(SOD^{M2}H(1)A)$[27]. A very weak high energy transition is also observed at 746 nm (28 M^{-1} cm^{-1}).

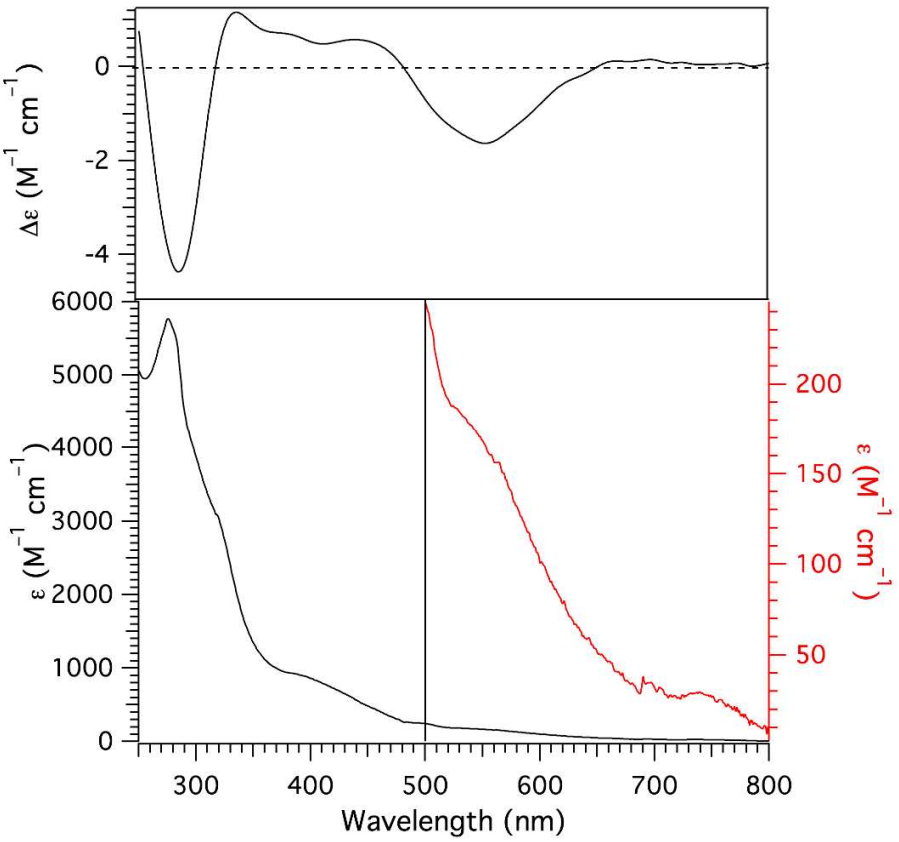

Figure 3.11 Electronic absorption spectrum (bottom) and CD spectrum (top) of {$Ni^{II}(H_2ase^{M2}$-Asp)}. Inset (red trace) depicts the expanded spectrum from 500 nm to 800 nm.

The CD spectrum displays positive features at 330 nm (Δε = 1.2 M^{-1} cm^{-1}), 385 nm (Δε = 0.68 M^{-1} cm^{-1}) and 445 nm (Δε = 0.58 M^{-1} cm^{-1}). An additional negative transition is observed at 555 nm (Δε = -1.6 M^{-1} cm^{-1}). The observed features are consistent with nickel-coordination to the peptide in either a square pyramidal or distorted tetrahedral geometry.[6,19] It should be noted that his is not entirely consistent with the ^{31}PNMR spectrum, which suggested a low-spin Ni(II)

center is present. It is possible that the NMR spectrum displayed a small concentration of a low-spin Ni(II) species in a square planar environment.

3.4.6 X-ray Absorption Studies of {$Ni^{II}(H_2ase^{M1})$}

To gain further insight into the geometry about the Ni-center of {$Ni^{II}(H_2ase^{M1})$}, Ni K-edge X-ray absorption spectra were collected at the National Synchrotron Light Source at Brookhaven National Lab (Upton, NY) (Fig. 3.13). The X-ray absorption near-edge (XANES) region of the X-ray absorption spectrum was found to be most consistent with either a square pyramidal or highly distorted tetrahedral coordination geometry. The lack of a square planar coordination motif as indicated by the electronic absorption spectra is confirmed by the absence of a well-defined Ni 1s $\rightarrow$ 4pz transition at ~8338 eV. Instead, an unresolved Ni 1s $\rightarrow$ 4p transition at 8339.6 eV can be observed, which is consistent with either a square pyramidal or tetrahedral Ni-center. Furthermore, a reasonably intense Ni 1s $\rightarrow$ 3d transition can be observed at 8331.9 eV (area = 7.2% eV relative to the edge height). This is inconsistent with square-planar Ni(II) complexes, which display weak Ni 1s $\rightarrow$ 3d transitions resulting from centrosymmetric ligand geometry. The observed intensity is instead consistent with either square pyramidal or tetrahedral geometries, as the intensity is between that observed for both geometry types.

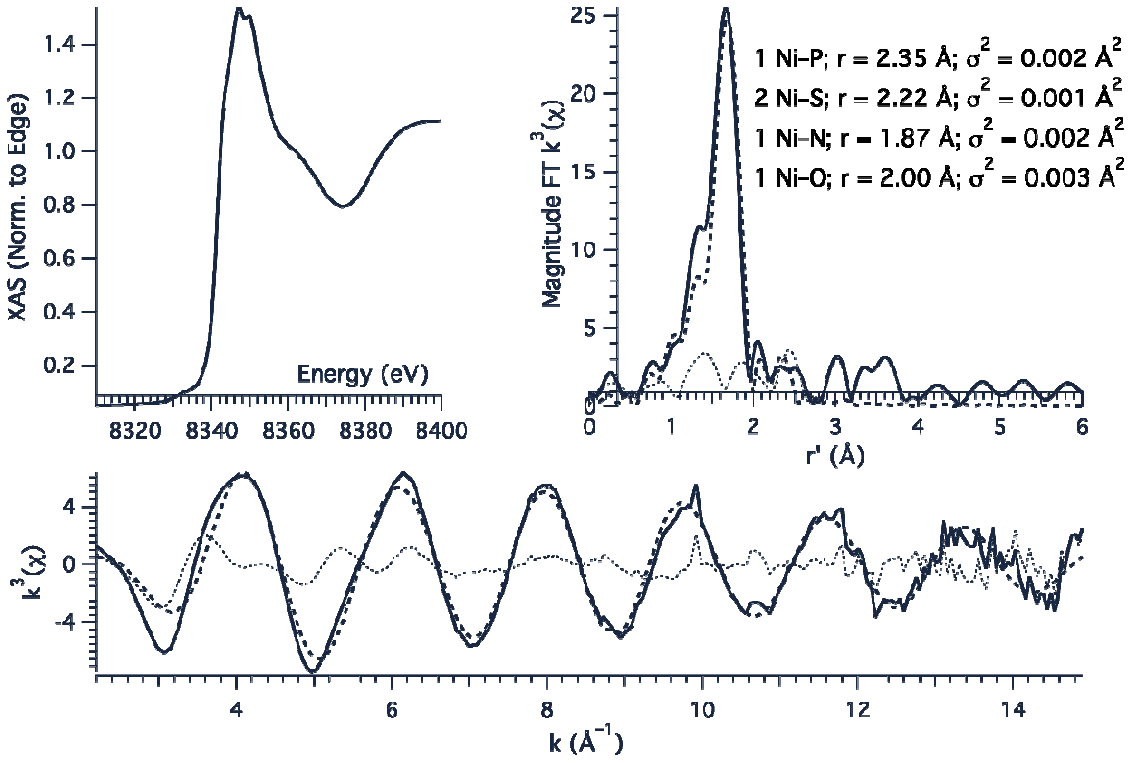

Figure 3.12 Top left: XANES region of the Ni K-edge X-ray absorption spectrum of {$Ni^{II}(H_2ase^{M1})$}. Top right: Magnitude Fourier transformed Ni K-edge EXAFS spectrum of {$Ni^{II}(H_2ase^{M1})$} depicting the experimental data (solid line), simulation to the data (dashed line), and difference spectrum (dotted line). Bottom: k3 EXAFS Ni K-edge EXAFS spectrum of {$Ni^{II}(H_2ase^{M1})$} depicting the experimental data (solid line), simulation to the data (dashed line), and difference spectrum (dotted line). Shell #1: 1 Ni–P, r = 2.348(3) Å, σ2 = 0.0022(1) Å2; Shell #2: 2 Ni–S, r = 2.222(3) Å, σ2 = 0.0008(3) Å2; Shell #3: 1 Ni–N, r = 1.86(1) Å, σ2 = 0.0024(1) Å2; Shell #4: 1 Ni–O, r = 2.000(4) Å, σ2 = 0.0024(1) Å2; Eo = 8341.6 eV; ε2 = 0.81.

The X-ray absorption far-edge (EXAFS) data, which are most consistent with a square pyramidal Ni-center, support the conclusions drawn from XANES analysis. The EXAFS region of the Ni K-edge X-ray absorption spectrum was best modeled as a five coordinate nickel center with: two sulfur-based ligands at 2.22 Å, one phosphorous-based ligand at 2.35 Å, one nitrogen-based ligand at 1.86 Å, a single N/O-based ligand at 2.00 Å (Fig. 3.14). These data are consistent with a square pyramidal geometry. However, if one considers a mixture of coordination

geometries, as indicated by the ^{31}PNMR spectrum and electronic absorption spectrum, it is possible that the EXAFS data is reflecting a mixture of the two complexes.

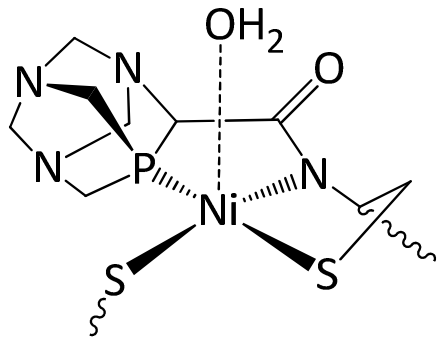

Figure 3.13 Proposed coordination environment of {$N^{II}I(H_2ase^{M1})$} based XAS experiments.

3.5 Origin of the Two Coordination Geometries

Upon observation of the electronic absorption and, more importantly, the X-ray absorption spectra, it is evident that the metallation of the {H_2ase^{M2}-Asp} apopeptide resulted in a mixture of Ni(II)-metallopeptide species with low-spin square pyramidal and high-spin distorted-tetrahedral geometries. This mixture of geometries may be a result of the chiral nature of the *N*-terminal PTA which contains a stereogenic carbon α to the coordinated phosphorus atom and its coupling to the peptide as a racemic mixture. Subsequently, one enantiomer is suggested to force planarity of the acyl-linker between the coordinated phosphorus and amidate-nitrogen atoms, effectively increasing the bite angle and resulting in an overall distorted tetrahedral geometry. The other enantiomer is proposed to push the acyl linker out plane with the rest of the chelating ligand set, allowing for a decreased bite angle and a more planar ligand sphere about the nickel center (Fig. 3.14). Using crystal field arguments it can be rationalized that the square pyramidal metallopeptide is observed in the ^{31}PNMR spectrum while the presence of the high-spin distorted-tetrahedral Ni(II) complexes goes

unnoticed. This also explains the very weak low energy transition in the UV-Vis spectrum, which is in agreement with the mixture of geometries found in the CD and XAS data.

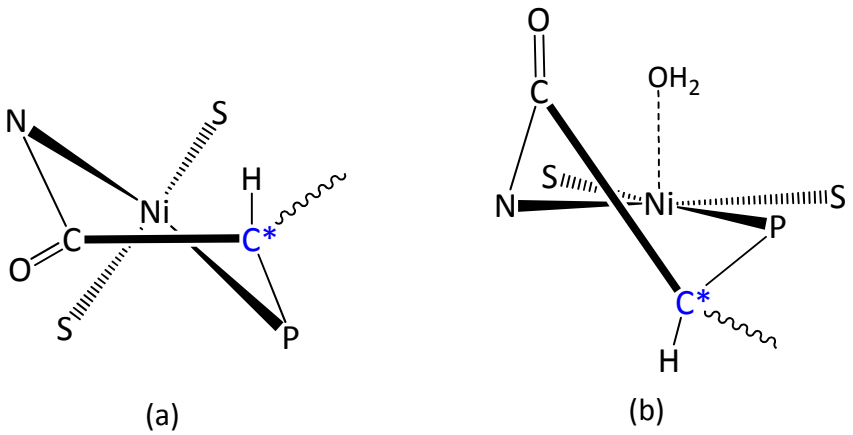

Figure 3.14 (a): High-spin tetrahedral coordination environment suggested from CD and XAS data; (b): low-spin square pyramidal coordination environment suggested by XAS and ^{31}PNMR data.

3.6 Conclusions

The purpose of this study was to modify a known metallopeptide mimic consisting of the 12 *N*-terminal residues including the NiSOD binding hook region in order to functionalize the active site for H_2 production. It has been demonstrated previously that axial coordination of the *N*-terminal histidine residue to the nickel center is not required for coordination of the apopeptide.[27] The amidate moiety was found to be essential for nickel coordination to the apopeptide[22] in addition to providing oxidative stability to coordinated thiolates[23,24]. Additionally the presence of thiolate coordination is a common trait shared by NiSOD and the nickel center in [NiFe]H_2ase. [6,25,26] The functionality of thiolates as internal bases in the NiSOD^{M1} metallopeptide has been implicated in proton transfer during oxidation of the nickel center, suggesting the possibility of proton shuttling from solvent to form Ni-hydride species as in other functional H_2ase models.[20,21] It was found that substitution of the *N*-terminal histidine residue

with a carboxylate-functionalized PTA through solid-phase peptide synthesis procedures resulted in coordination of nickel upon addition of one equivalent of $NiCl_2$ to a buffered solution containing the apopeptide.

Electronic absorption experiments display weak features in the ligand-field region (321, 385, 503, and 541 nm) with the absence of a band near 460 nm, which is a characteristic feature of the $Ni(3d_{x2-y2}/S(\pi)^* \rightarrow Ni(3d_{x2-y2}/S/N(\sigma))^*$ transition observed in $Ni^{II}N_2S_2$ complexes including $NiSOD^{M1}$ and the native enzyme.[6,19,27] An additional weak feature in the near-IR region is suggestive of a deviation from the square planar geometry observed in previously reported NiSOD maquettes.[6,19,27] The CD spectrum provides further evidence for coordination of the nickel center within a chiral environment.

XAS studies of the Ni K-edge provide evidence for either a 5 coordinate square pyramidal geometry involving axial coordination of a water molecule or a distorted tetrahedral geometry about the nickel-center. XANES experiments display an edge feature 8339.6 eV) shifted higher in energy from previously reported square planar NiN_2S_2 metallopeptides (8338 eV)[19,27]. Furthermore, inter-atom bond distances derived from the EXAFS region display amidate, bis-thiolate and phosphorus ligation, confirming successful coupling of the PTA functionality to the apopeptide as well as successful coordination to the nickel center. Additionally the Ni-S bond lengths are elongated by ~0.04 Å relative to square planar Ni cis-thiolate compounds our group has previously probed and is consistent with an increase in nickel-center coordination number.[19] The short Ni-N bond length is consistent with anionic amidate nitrogen coordination, while the longer oxygen donor may be derived from a water molecule. Thus, we propose that $\{N^{II}I(H_2ase^{M1})\}$ contains Ni(II) within a square-pyramidal coordination environment with an axial ligand derived from water and equatorial ligands

derived from the PTA phosphorous atom, the two cysteinate sulfur atoms, and the Cys(2) amidate nitrogen atom.

In an attempt to quantify the ability of this modified metallopeptide to produce H_2, future electrochemical studies will be performed by tethering both the {$Ni^{II}(H_2ase^{M2}$-Asp)} and {$Ni^{II}(H_2ase^{M2}$-Lys)} metallopeptides directly to a pyrolytic graphite electrode. Monitoring of the headspace for H_2 upon reduction in the presence of a suitable proton donor should allow the functionality of this new model H_2ase to be determined.

3.7 References

1) Phillips, A. D.; Gonsalvi, L.; Romerosa, A.; Vizza, F.; Peruzzini, M. *Coord. Chem. Rev.* **2004**, *248*, 955-993 and references within

2) (a) Daigle, D. J.; Darensbourg, D. J. Inorganic Synthesis; John Wiley & Sons: Published Online 5, Jan, 2007; Print ISBN: 9780471249214; Online ISBN: 9780470132630; DOI: 10.1002/9780470132630
(b) Daigle, D. J.; Darensbourg, M. Y. *Inorg. Chem.* **1975**, *14*, 1217=1218
(c) Delerno, J. R.; Trfonas, L. M.; Darensbourg, M. Y.; Majeste, R. J. *Inorg. Chem.* **1976**, *15*, 812-816

3) Frost, B. J.; Wong, G. W.; Lee, W. *Inorg. Chem.* **2008**, *47*, 612-620

4) Hegg, E. L.; Shearer, J.; Mathrubootham, V.; Thomas, J.; Stables, R.; McCraken, J. *Inorg. Chem.* **2010**, *49*, 5393-5406

5) Shearer, J.; Dehestanl, A.; Abanda, F. *Inorg. Chem.* **2008**, *47*, 2649-2660

6) Brunold, T. C.; Fiedler, A. T.; Bryngelson, P. A.; Maroney, M. J. *J. Am. Chem. Soc.* **2005**, *127*, 5449-5462

7) Getzoff, E. D.; Barondeau, D. P.; Kassmann, C. J.; Bruns, C. K.; Tainer, J. A. *Biochemistry*, **2004**, *43*, 8038-8047

8) Maroney, M. J.; Ryan, K. C.; Johnson, O. E.; Cabelli, D. E.; Brunold, T. C. *J. Biol. Inorg. Chem.*, **2010**, *15*, 795-807

9) Maroney, M. J.; Bryngelson, P. A.; Arobo, S. E.; Pinkham, J. L.; Cabelli, D. E. *JACS*, **2004**, *126*, 460-461

10) Peruzzini, M.; Phillips, A. D.; Gonsalvi, L.; Romerosa, A.; Vizza, F. *Coord. Chem. Rev.*, **2004**, *248*, 955-993

11) (a) Fontecilla-Camps, J. C.; Volbeda, A.; Cavazza, C.; Nicolet, Y. *Chem. Rev.* **2007**, *107*, 4273-4303
(b) Collman, J. P. *Nat. Struct. Biol.* **1996**, *3*, 213-222
(c) Bagley, K. A.; Van Garderen, C. J.; Chen, M.; Duin, E. C.; Albracht, S. P.; Woodruff, W. H. *Biochemistry* **1994**, *33*, 9229-9236
(d) Bagley, K. A.; Duin, E. C.; Roseboom, W.; Albract, S. P. J.; Woodruff, W. H. *Biochemistry*, **1995**, *34*, 5527-5535
(e) Happe, R. P.; Roseboom, W.; Pierik, A. J.; Albracht, S. P. J.; Bagley, K. A. *Nature*, **1997**, *385*, 126

12) Varganov, S. A.; Yson, R. L.; Gilgor, J. L; Guberman, B. A. *Chem. Phys. Lett.* **2013**, *577*, 138-141

13) (a) Artero, V.; Canaguier, S., Fourmond, V.; Perotto, C. U.; Fize, J.; Pecaut, J.; Fontecave, M.; Field, M. J. *Chem. Comm.* **2013**, *49*, 5004-5006
(b) Artero, V.; Fontecave, M.; Canaguier, S.; Field, M.; Oudart, Y.; Pecaut, J. *Chem. Comm.* **2010**, *46*, 5876-5878

14) DuBois, D. L.; DuBois, M. R. *Chem. Soc. Rev.*, **2009**, *38*, 62-72

15) Ogo, S. *Chem. Comm*. **2009**, *23*, 3317-3325

16) Bullock, R. M.; DuBois, D. L. *Eur. J. Inor. Chem.* **2011**, 1017-1027

17) Shearer, J.; *Angew. Chem. Int. Ed.*, **2013**, *52*, 2569-2572

18) Baffert C.; Sybirna, K.; Ezanno, P.; Lautier, T.; Hajj, V.; Meynial-Salles, I.; Soucaille, P.; Bottin, H.; Leger, C. *Anal. Chem.* **2012**, *84*, 7999-8005

19) Shearer, J.; Zhao, N. *Inorg. Chem.* **2006**, *45*, 9637-9639

20) DuBois, D. L.; DuBois, M. R.; Wilson, A. D.; Newell, R. H.; McNevin, M. J.; Muckerman, J. T. *JACS* **2006**, *128*, 358-366

21) Ogo, S. *Chem. Comm*. **2009**, *23*, 3317-3325

22) Shearer, J.; Unpublished Data

23) Brunold, T. C.; Fiedler, A. T.; Bryngelson, P. A.; Maroney, M. J. *J. Am. Chem. Soc.* **2005**, *127*, 5449-5462

24) Shearer, J.; Dehestanl, A.; Abanda, F. *Inorg. Chem.* **2008**, *47*, 2649-2660

25) Fontecilla-Camps, J. C.; Volbeda, A.; Cavazza, C.; Nicolet, Y. *Chem. Rev.* **2007**, *107*, 4273-4303

26) Voldbeda, A.; Charon, M.; Piras, C.; Hatchikian, E. C.; Frey, M.; Fontecilla-Camps, J. C. *Nature* **1995**, *373*, 580-587

27) Shearer, J.; Neupane, K. P.; Gearty, K.; Francis, A. *J. Am. Chem. Soc.* **2007**, *129*, 14605-14618

Chapter 4

Methods

4.1 Chemicals Used

All amino acids used featured Fmoc protecting groups without further protection with the exception of the following whose side chains featured additional protecting groups: Asp (oBut), Tyr (But) Cys (Trt). All amino acids and Paramax Wang resin (200-400 mesh, 1.0 mmol/g) were purchased from Advanced Chem Tech and stored at 0°C. Dichloromethane, diethyl ether and tetrahydrofuran were distilled from CaH_2, $LiAlH_4$, and NaK amalgam/ benzophenone, respectively, under nitrogen. 1,3,5-triaza-7-phosphatricyclo[3.3.1.1]decane (PTA) was prepared according to literature procedures in air.[1-3] All subsequent reactions in the synthesis of PTA-COOLi were performed in a nitrogen atmosphere using Schlenk line techniques. All other reagents were obtained from Sigma-Aldrich and used as received.

4.2 PTA-COOLi Synthesis

The procedure published by Frost was followed. 922 mg PTA was used as obtained from the Frost group without further purification, was suspended in THF in a Schlenk flask, subsequently sparged with nitrogen and cooled in a dry ice/ acetone bath. To the suspension was added 1.3 equivalents 2.0 M butyllithium solution in cyclohexane over approximately 20 minutes and the solution was allowed to stir under nitrogen for four hours. The crude mixture was then filtered under nitrogen using a sinter (glass frit) to afford an off-white pyrophoric solid, which was subsequently washed with dry hexanes, suspended in THF and transferred to a Schlenk flask. The solution was again cooled in a dry ice/ acetone bath and CO_2 (g) was allowed to bubble through the reaction mixture for five hours. Subsequent washing of crude PTA-COOLi with CHCl3 and centrifugation afforded 875 mg of purified product (72% yield). The off-white solid

was characterized by ^{1}HNMR (500 MHz, D_2O): 4.50-4.21 (m, 6H, NC*H*$_2$N); 3.90 (m, 1H, PC*H*N); 3.75-3.63 (m, 4H, PC*H*$_2$N) and ^{31}PNMR (162 MHz, D_2O): -90.1 (s).

4.3 Peptide Synthesis

All PTA-containing peptides (H_2ase^{M1}, PTA-CDLPC-GVYDP-A-COOH; H_2ase^{M2}-Asp/Lys, PTA-CDLPC-GVYDP-A(D/K)-COOH) were synthesized utilizing Fmoc (9-fluoromethoxycarbonyl) chemistry following standard solid phase peptide synthesis (SPPS) procedures.[5-7] 100 mg of ParaMax Wang resin was swelled in dichloromethane (DCM) for one hour in a peptide reactor and the first *C*-terminal amino acid (AA1) was added using the anhydride method. Synthesis of the anhydride was accomplished by first dissolving 10 equivalents of AA1 in DCM and minimal dimethyl formamide (DMF) followed by addition of N,N'-diisopropylcarbodiimide (DIC) under N_2 at 0°C. This solution was stirred for 40 minutes and brought to room temperature after which all volatiles were removed *in vacuo*. The resulting residue was dissolved in DMF and a single small crystal of 4-N,N-dimethylaminopyridine (DMAP) was added before addition to the resin. After shaking for one hour on a wrist action shaker the solution was washed five times with 1-2 mL DMF (the peptide is washed with DMF after every agitation step unless otherwise noted) and the addition of AA1 anhydride was repeated. The remaining coupling sites on the resin were then capped by addition of five equivalents of benzoic anhydride and a few drops of pyridine in DMF followed by agitation for 30 minutes.

Following addition of AA1 to the resin an Fmoc deprotection step was performed upon addition of 1-2 mL 20% piperidine solution in DMF followed by agitation for 20 minutes. Subsequent amino acids (five equivalents of each relative to resin loading; mmol/g) were added to the deprotected peptide chain by dissolving in minimal DMF (dimethylformamide) with the coupling reagents HBTU (*O*-(benzotriazol-1-yl)-*N,N,N',N'*-tetramethyluronium

hexafluorophosphate), HOBt (hydroxybenzotriazol) and DIPEA (diisopropylethylamine), followed by shaking for one hour. Deprotection of aspartic acid residues included 0.1M HOBt in the deprotecting solution to avoid aspartamide formation. After addition and deprotection of the Cys(2) AA, 10 equivalents of PTA-COOLi were dissolved in minimal DMF upon addition of 3 drops dimethylsulfoxide (DMSO) and 2 drops pyridine. This solution was added to the deprotected peptide, coupled for three hours. This process was performed in triplicate to ensure coupling of the PTA functionality to the apopeptide.

Once all of the residues had been coupled, the peptide was cleaved from the resin by washing with methanol followed by DCM and removal of volatiles *in vacuo*. A cleaving solution ("Reagent K"; 82.5% trifluoroacetic acid (TFA), 2.5% ethanedithiol, 5% thioanisol, 5% phenol, 5% H_2O) was added to the dried resin and allowed to sit for five hours, after which the resin was removed via filtration through glass wool and washed with TFA. The resulting peptide was concentrated by removal of volatiles under vacuum and crashed out with cold diethyl ether and isolated after repeated washing and centrifugation.

4.4 Peptide Purification

Purification of peptides was achieved using reverse phase HPLC on a Waters DeltaPrep-600 utilizing a Waters X-Bridge C-18 column (30 x 150 mm; 5 µm) and a 10-29% MeCN (0.1%) TFA in H_2O (0.1% TFA) mobile phase gradient over 15 minutes. Fractions were collected at 13.32 {H_2ase^{M1}}, 13.20 {H_2ase^{M2}-Asp} and 12.92 {H_2ase^{M2}-Lys} and lyopholized yielding a white solid: 13 mg (9.7% yield) {H_2ase^{M1}}; 6 mg (4% yield) {H_2ase^{M2}-Asp}; 35 mg (20.8% yield) {H_2ase^{M2}-Lys}). Analytical reverse phase HPLC on a Waters DeltaPrep 600 and Waters X-Bridge C-18 column (4.5 x 150 mm; 5 µm) employed a 10-65% MeCN (0.1% TFA) in H_2O (0.1% TFA) mobile phase gradient

over 65 minutes with a flow rate of 1 mL/ min to determine peptide purity with retention times at 17.27 {H_2ase^{M1}}, 17.99 {H_2ase^{M2}-Asp} and 18.02 {H_2ase^{M2}-Lys}.

4.5 Nickel(II) Coordination to the Metallopeptides

Peptides {H_2ase^{M1}} and {H_2ase^{M2}-Asp} were dissolved in nitrogen-sparged 50 mM N-ethylmorpholine buffer (NEM; pH 8.0). The free thiol concentration of the isolated peptide was accurately determined using the Ellman's Assay . Addition of Ellman's solution (50 mM NaOAc, 2 mM Ellman's reagent) and 1.0 M Tris buffer (pH 8.0) to the peptide in a 1 cm quartz cuvette and subsequent inspection of the peak observed at 412 nm (ε_{412} = 13,600 M^{-1} cm^{-1}) in the UV-Vis spectrum yielding a peptide concentration of approximately 0.5 mM. A solution of $NiCl_2$ in degassed H_2O was prepared and one equivalent was added to a solution under anaerobic conditionscontaining the peptide in 50 mM NEM buffer resulting in the formation of a brown solution. UV-Vis (λ_{max}= 746 nm; ε= 28 M^{-1} cm^{-1}; λ_{max}= 541 nm; ε= 177 M^{-1} cm^{-1}; λ_{max}= 503 nm; ε= 239 M^{-1} cm^{-1}; λ_{max}= 385 nm; ε= 927 M^{-1} cm^{-1}; λ_{max}= 321 nm; ε= 2970 M^{-1} cm^{-1}; λ_{max}= 278 nm; ε= 5712 M^{-1} cm^{-1}) and CD experiments (λ_{max}= 555 nm; Δε= -1.6 M^{-1} cm^{-1}; λ_{max}= 445 nm; Δε= 0.58 M^{-1} cm^{-1}; λ_{max}= 385 nm; Δε= 0.68 M^{-1} cm^{-1}) were subsequently performed confirming Ni(II) coordination to the peptide in a chiral environment. All solutions were prepared under anaerobic conditions in a Coy chamber and samples prepared for XAS experiments were stored at 20 K.

4.6 General Instrumental Methods

NMR (nuclear magnetic resonance) experiments were performed on a Varian VNMRS 400 NMR spectrometer (^{1}HNMR) and 400-MR spectrometer (^{31}PNMR) using VNMRJ Version 2.3 Revision A software with chemical shifts reported in parts-per-million (ppm). UV-Vis spectra

were collected under anaerobic conditions on either a CARY 50 or Perkin-Elmer Lambda 750 UV-Vis-NIR spectrometer (1200 – 250 nm) using quartz cuvettes with 1 cm path length. Circular dichroism (CD) spectra were recorded on a Jasco J-715 spectropolarimeter using circular quartz cuvettes (800 – 250 nm; 1 data point per 0.05 nm) and represent the average of five scans. Each spectrum was collected as an average of 5 scans with buffer baseline subtracted from each spectrum.

4.7 References

1) Daigle, D. J.; Darensbourg, D. J. Inorganic Synthesis; John Wiley & Sons: Published Online 5, Jan, 2007; Print ISBN: 9780471249214; Online ISBN: 9780470132630; DOI: 10.1002/9780470132630

2) Daigle, D. J.; Darensbourg, M. Y. *Inorg. Chem.* **1975**, *14*, 1217

3) Delerno, J. R.; Trfonas, L. M.; Darensbourg, M. Y.; Majeste, R. J. *Inorg. Chem.* **1976**, *15*, 816

4) Frost, B. J.; Wong, G. W.; Lee, W. *Inorg. Chem.* **2008**, *47*, 612

5) Chan. W. C.; White, P. D. *Fmoc solid phase peptide synthesis: A practical approach*, Oxford University Press, USA.

6) Atherton, E.; Sheppard, R. C. *Solid phase peptide synthesis: a practical approach, Oxford University Press*; Oxford, New York, Tokyoa 1989.

7) Bodanszky, M. *Peptide chemistry: A practical testbook*; Springer-Verlag Berlin Heidelberg 1988.

8) Ellman, G. L. *Arch. Biochem. Biophys.* **1958**, *74*, 443